

UC Berkeley

UC Berkeley Previously Published Works

Title

A Förster Resonance Energy Transfer (FRET)-based System Provides Insight into the Ordered Assembly of Yeast Septin Hetero-octamers*

Permalink

<https://escholarship.org/uc/item/51r2j9bh>

Journal

Journal of Biological Chemistry, 290(47)

ISSN

0021-9258

Authors

Booth, Elizabeth A
Vane, Eleanor W
Dovala, Dustin
[et al.](#)

Publication Date

2015-11-01

DOI

10.1074/jbc.m115.683128

Peer reviewed

A Förster Resonance Energy Transfer (FRET)-based System Provides Insight into the Ordered Assembly of Yeast Septin Hetero-octamers

Elizabeth A. Booth^{1a}, Eleanor W. Vane^{1b}, Dustin Dovala^{2c} and Jeremy Thorner^{1*}

¹Division of Biochemistry, Biophysics, and Structural Biology, Department of Molecular and Cell Biology, University of California, Berkeley, CA 94720-3202

²Program in Microbial Pathogenesis and Host Defense, Department of Microbiology and Immunology, University of California School of Medicine, San Francisco, CA 94158-2200

Running title: *A spectroscopic approach for analysis of septin assembly*

*To whom correspondence should be addressed: Prof. Jeremy Thorner, Dept. of Molecular and Cell Biology, University of California, Rm. 526, Barker Hall, Berkeley, CA 94720-3202. Phone: (510) 642-2558, FAX: (510) 642-6420, E-mail: jthorner@berkeley.edu

Key Words: Fluorescence, *Saccharomyces cerevisiae*, protein self-assembly, protein engineering, Cdc11, Shs1, polymerization, protein-protein interactions

Background: Septins self-assemble into hetero-octameric rods and higher order structures and recruit other proteins.

Results: A spectroscopic method (FRET) to measure septin interactions and binding of associated proteins was developed.

Conclusions: End-to-end polymerization of Cdc11-capped rods, heterotypic end-to-end junctions between Cdc11-capped rods and Shs1-capped rods, and binding of an associated protein were demonstrated.

Significance: This spectroscopic assay provides new insights about these polymeric proteins.

Prior studies in both budding yeast (*Saccharomyces cerevisiae*) and in human cells have established that septin protomers assemble into linear hetero-octameric rods with two-fold rotational symmetry. In mitotically-growing yeast cells, five septin subunits are expressed (Cdc3, Cdc10, Cdc11, Cdc12 and Shs1) and assemble into two types of rods that differ only in their terminal subunit— Cdc11-Cdc12-Cdc3-Cdc10-Cdc10-Cdc3-Cdc12-Cdc11 and Shs1-Cdc12-Cdc3-Cdc10-Cdc10-Cdc3-Cdc12-Shs1. EM analysis has shown that, under low-salt conditions, the Cdc11-capped rods polymerize end-to-end to form long paired filaments, whereas Shs1-capped rods form arcs, spirals and rings. To develop a facile method to study septin polymerization *in vitro*, we exploited our previous work where we generated septin complexes in which all endogenous cysteine

(Cys) residues were eliminated by site-directed mutagenesis, except an introduced E294C mutation in Cdc11 in these experiments. Mixing samples of a preparation of such single-Cys containing Cdc11-capped rods that have been separately derivatized with organic dyes that serve as donor and acceptor, respectively, for FRET provided a spectroscopic method to monitor filament assembly mediated by Cdc11-Cdc11 interaction and to measure its affinity under specified conditions. Modifications of this same FRET scheme also allow us to assess whether Shs1-capped rods are capable of end-to-end association either with themselves or with Cdc11-capped rods. This FRET approach also was used to follow the binding to septin filaments of a septin-interacting protein, the type II myosin-binding protein Bni5.

Septins are a family of GTP-binding proteins found in all eukaryotes (except plants) (1,2), and have roles in cytokinesis, cell compartmentation, and membrane remodeling (3-5). The *S. cerevisiae* genome encodes five septins that are expressed in mitotically-growing cells: Cdc3, Cdc10, Cdc11, Cdc12, and Shs1 (6,7). Four of these proteins were first identified because the corresponding loci were among the temperature-sensitive (ts) cell division cycle (*cdc*) mutations isolated by Hartwell and co-workers and specifically exhibited failure of cytokinesis at the restrictive temperature (8,9). The fifth member was identified later by other

means and recognized as a gene product homologous to the other four (10,11).

During initial characterization of the *cdc* mutants by EM³, it was noted that, after incubation of cells at the restrictive temperature, the *cdc3*, *cdc10*, *cdc11* and *cdc12* mutants uniquely lost filament-like striations found at the bud neck in control cells (12). These striations were 10 nm wide and approximately 28 nm apart. Indirect immunofluorescence with anti-septin antibodies (13-15) and, later, fusion of septins to fluorescent proteins (16,17), demonstrated that septins are located at and likely constituents of the filamentous bud neck structure. Subsequently, purification of septins from yeast (18), and as recombinant proteins from bacteria (19-21), showed that Cdc3, Cdc10, Cdc11, and Cdc12 were sufficient to form long-paired filaments *in vitro* (22) that closely resemble those seen by EM at bud neck *in vivo* (12,23,24).

Ensuing work showed that the five mitotic septins of yeast form two types of linear, apolar hetero-octameric complexes of a defined order, which differ only with respect to the terminal subunit present: Cdc11-Cdc12-Cdc3-Cdc10-Cdc10-Cdc3-Cdc12-Cdc11 and Shs1-Cdc12-Cdc3-Cdc10-Cdc10-Cdc3-Cdc12-Shs1 (22,25). These two types of rods are very stable, even in high salt (≥ 250 mM) buffers. When the salt concentration is reduced (< 100 mM), Cdc11-capped rods polymerize end-to-end into long paired filaments, as visualized *in vitro* by EM (22) and by super-resolution fluorescence microscopy (26). By contrast, Shs1-capped rods associate laterally in a staggered manner generating bundles that interact to form arcs, spirals and rings (25). The septin collar at the bud neck appears to have three primary functions: (i) it establishes a cortical diffusion barrier (27,28); (ii) it serves as a scaffold to recruit other proteins (29,30); and, (iii) it promotes membrane curvature either directly by deforming the membrane and/or indirectly by recruiting other proteins that can remodel membranes (31-33).

As for yeast, members of the family of 13 human septins also form linear hetero-octameric rods, the most abundant of which has the composition Sept9-Sept7-Sept6-Sept2-Sept2-Sept6-Sept7-Sept9 (34,35). Moreover, crystal structures of individual human septins (36,37) or septins from other animal cells (38),

and of a human hetero-hexameric complex (39,40), revealed the nature of the two alternating interfaces that mediate linear assembly of the protomers into the hetero-oligomeric rod. The G interface between two subunits is an *en face* interaction that involves residues in and around the GTP-binding pockets of each protomer; and, at the opposing surface (180° away from the G interface), is the NC interface wherein two subunits associate via contacts provided by residues in and around the N- and C-terminal segments of each protomer (39). Biochemical analysis (19,41) and structural studies (38,40) have shown how GTP binding, and, in the case of certain septin subunits, GTP hydrolysis, influences subunit conformation and interaction. In the yeast hetero-octamer, the Cdc11-Cdc12 interface is a G interface, the Cdc12-Cdc3 interface is an NC interface, and so forth (Fig. 1A). Aside from their globular GTP-binding fold, the yeast mitotic septins have N-terminal extensions of variable length, with Cdc11 the shortest (12 residues) and Cdc3 the longest (110 residues), and, with the exception of Cdc10, also possess a long (≥ 100 residue) flexible C-terminal extension (CTE) that contains a segment (~ 40 residues) with a strongly predicted propensity for coiled-coil formation (20,42).

To date, septin function *in vivo* has been studied primarily using genetic methods and septin properties *in vitro* have been studied largely by examining static structures under the EM. Fluorescence microscopy has been used to visualize septin polymerization, but due to the large dimensions of the fluorophores used, either antibodies for immunostaining (20) or fusions to GFP (43) or to the SNAP tag (44), and the diffraction limit of light, such approaches cannot address the molecular details of the mechanism of septin assembly. Furthermore, given the dimensions of the yeast septin hetero-octamer (4×32 nm), even super-resolution fluorescence microscopy applied to yeast septin filaments has merely confirmed what is already known about the order of subunits in the hetero-octamer (26).

To understand other self-assembling biopolymers, such as formation of microtubules from tubulin (45,46) and of F-actin from G-actin (47,48), and the interaction of these cytoskeletal elements with other proteins that bind to them, it has been exceedingly valuable to have spectroscopic assays to monitor the state of assembly in

real time under conditions that can be readily manipulated. For the purposes of interrogating interactions at the protein-protein level, Förster resonance energy transfer (FRET) is especially well suited. FRET allows for rapid measurements, is sensitive to the distance between the donor and acceptor fluorophores at the ≤ 10 nanometer scale, and the donor-acceptor/quencher interaction provides an unambiguous indication of how two elements within the system under study are associating. Given the hetero-oligomeric nature of septin complexes, we felt that FRET could provide a robust and sensitive means to investigate under a wide range of experimental conditions important, and heretofore inaccessible, mechanistic details about the dynamics and affinities of the protein-protein interactions involved in assembly and organization of septin structures.

Here we describe our development of a reliable FRET-based system for studying the polymerization of septin complexes into filaments, the effects of ionic strength on septin filament assembly, the interplay between Cdc11- and Shs1-capped hetero-octamers, the effects of mutational perturbation of important structural elements in the protomers on their ability to assemble, and the binding of a septin-associated protein. Our findings have important implications for understanding the physiological roles of alternate septin subunits and how septins behave as a polymeric system.

EXPERIMENTAL PROCEDURES

Expression and purification of septin complexes—Septin subunits were co-expressed from two DUET™ vectors (EMD Millipore) with compatible origins of replication essentially as described previously (20), except that *Escherichia coli* NiCo21 (DE3) (New England Biolabs) was used as the production strain because it has been engineered to prevent recovery of GlnS and several other endogenous *E. coli* Ni²⁺ bead-binding proteins that are normally major contaminants in purifications utilizing IMAC (49). Prior work from this laboratory demonstrated that the Cys-less septins Cdc3(C124V C253V C279V), Cdc10(C266S), Cdc11(C43F C137A C138A), (His)₆-Cdc12(C40A C278S) and Shs1(C29V C148S) supported yeast cell viability and formed recombinant hetero-octameric complexes that were

indistinguishable in their *in vitro* assembly properties from those produced from their wild-type counterparts (50). Using a combination of standard site-directed mutagenesis (51) and sequence and ligation independent cloning ("SLIC") (52), derivatives of each of the Cys-less septins were constructed in which a single Cys was reinstalled at a selected position. A pACYC plasmid expressing Cdc3(C124V C253V C279V) and Cdc11(C42F C137A C138A E294C Δ 303-415) (50) was repaired to restore an intact CTE (residues 303-415) to the *CDC11* ORF. A pACYC plasmid that expresses Cdc3(C124V C253V C279V) and Shs1(C29V C148S E344C) was constructed for production and purification of Shs1-capped hetero-octamers. Bacterial cultures were grown to an $A_{600nm} = 0.8 - 1.0$, induced with isopropyl- β -D-thiogalactoside (0.5 mM final) overnight at 16°C, collected by centrifugation and resuspended in ice-cold lysis buffer [300 mM KCl, 40 μ M GDP, 0.1% monothioglycerol, 0.5% Tween-20, 12% glycerol, 20 mM imidazole, 50 mM Tris-HCl (final pH 8.0) plus protease inhibitor mix (Complete EDTA-free, Roche, Basel) and 0.2 mg/mL lysozyme]. Cells were ruptured at 4°C by six 15-sec pulses of sonic irradiation using a Branson Cell Disrupter (Model W185D), separated by 15-sec periods of cooling. The resulting lysate was clarified by centrifugation at 10,000g for 30 min at 4°C. The clarified extract was subjected to IMAC on Ni²⁺-NTA agarose beads (Qiagen) in high-salt buffers [wash buffer: 300 mM KCl, 20 mM imidazole, 50 mM Tris-HCl (final pH 8.0); elution buffer: 300 mM KCl, 500 mM imidazole, 50 mM Tris-HCl (final pH 8.0)]. Fractions containing the bulk of the purified septin complexes were combined and the resulting pool (typically 5-6 mL) was passed over chitin-agarose beads (New England BioLabs) to remove three other endogenous *E. coli* gene products (ArnA, SlyD and Can) that are other known contaminants in IMAC-based purifications [because, in *E. coli* NiCo21 (DE3), each of these gene products has been tagged with a chitin-binding domain]. The septin complexes in the flow-through from the chitin-agarose were loaded using the 10-mL loop of an AKTA FPLC system (GE Healthcare) onto a Superdex 200 HiLoad 16/60 column (16 mm x 60 cm) (GE Healthcare) and subjected to size-exclusion chromatography in septin buffer [300 mM KCl, 50 mM Tris-HCl (final pH 8.0)]. Fractions were collected, and the proteins present in

each were resolved by SDS-PAGE and visualized by staining with Coomassie Blue dye. The peak fractions containing the highest concentrations of stoichiometric septin complexes were pooled and used immediately for labeling by maleimide chemistry.

Expression and purification of Bni5—Using the SLIC procedure, the yeast *BNI5* ORF was inserted in-frame with an N-terminal 8XHis tag followed by a human rhinovirus 3C protease cleavage site in the bacterial expression vector pH3c-LIC, in which transcription is driven by the phage T7 promoter and regulated in an IPTG-dependent manner by a *lacO* element. This vector was introduced into *E. coli* NiCo21 (DE3), and the cells were induced and lysed, and the Bni5 protein purified by IMAC, chitin-agarose and size-exclusion chromatography, essentially as described above for the bacterially-expressed septin complexes.

Maleimide labeling—The protein concentration of the purified septin complexes (or Bni5) was determined using the bicinchoninic acid method (Pierce BCA protein assay kit; Life Technologies) (53). Samples (typically, 2-4 μ g) were incubated with a 10-fold molar excess of reducing agent TCEP for 10 min at room temperature, desalted by passage through Sephadex G25 (8.3 mL; PD-10 column, GE Healthcare) in labeling buffer [300 mM KCl, 50 mM Tris (final pH 7.0)] to remove the TCEP, and labeled overnight at 4°C with a 5-fold molar excess of the desired maleimide dye (AF488, AF555, AF647; Life Technologies). Excess dye was reacted with a 10-fold molar excess of DTT at room temperature for 10 min and removed by recapturing the (His)₆-Cdc12-containing septin complex by IMAC chromatography on a HisTrap HP column (GE Healthcare) [wash buffer: 300 mM KCl, 20 mM imidazole, 50 mM Tris-HCl (final pH 8.0); elution buffer: 300 mM KCl, 500 mM imidazole, 50 mM Tris-HCl (final pH 8.0)]. The dye-labeled protein was dialyzed overnight against septin buffer [300 mM KCl, 50 mM Tris-HCl (final pH 8.0)] in a Slide-A-Lyzer dialysis cassette (Life Technologies) with a 10 kDa molecular weight cut-off. The BCA assay (corrected for the contribution of the dye) and measurement of fluorescence using a P-330 Nanophotometer (Implen) were used to determine the molar concentration of protein and dye, respectively, in the final sample. In these complexes, in which only a

single protomer type, *e.g.* Cdc11, contains the sole Cys present, the efficiency of labeling was 0.7-0.8 dye molecules per this subunit. Labeling of only the proper protomer was verified by resolving the subunits by SDS-PAGE and analyzing them by imaging with a Typhoon Trio Variable Mode Imager equipped for fluorescence (GE Healthcare) to detect the dye and by staining with Coomassie blue dye and examining with an Odyssey scanner (Licor Biosciences) to detect the protein. Using the same criteria, the labeling efficiency for Bni5, which contains 3 native Cys, was 2.7 dye molecules per protein.

Spectroscopy and data analysis—Absorbance spectra of 25 nM donor dye (AF555)-labeled septin hetero-octamers alone, serial dilutions of 100 nM acceptor dye (AF647)-labeled septin hetero-octamers alone (unless otherwise specified), and mixtures of the two were measured, in triplicate, at room temperature after equilibration for 1 h in a cuvette (3-mm path length, 270 μ L maximum volume) using a Cary Eclipse Fluorescence Spectrophotometer (Agilent). Unless specified otherwise, the final buffer conditions were 45 mM KCl, 50 mM Tris-HCl (pH 8.0). FRET values were obtained by subtracting the buffer only background and correcting the emission of the acceptor at 671 nm for the contributions of both the donor and acceptor excited at 555 nM. The values reported represent the average (\pm SEM) of the triplicate samples. PCA (54) and subsequent data fitting was done using Matlab (The Mathworks) and its toolboxes for curve fitting and statistics. Alternately, semi-quantitative sensitized emission techniques were used to obtain corrected FRET values, as previously described (55-57).

Fluorescence microscopy—Microscope slides (3 inch x 1 inch x 1 mm) and coverslips (#1.5, 22 mm x 22 mm) were bathed in 2 M HCl for 30 min, rinsed 5 times in ddH₂O (15 min per wash) and once in ethanol, and air dried. To coat the coverslip, 300 μ L of 1 mg/mL PLL was pipetted onto its surface and after incubation for 30-60 min, it was rinsed 2 times with ddH₂O and air dried. Purified septin complexes labeled with AF488 and AF555, respectively, were mixed and diluted to final concentration of 20 nM in 45 mM KCl, 50 mM Tris-HCl (pH 8.0) and incubated for 1 h at room temperature while protected from light. Samples (30 μ L) of the

resulting septin filament-containing solution were pipetted onto the coverslip and followed immediately by 200 μ L of the same buffer to help disperse the protein more uniformly. The filaments were allowed to adhere to the PLL surface for 30 min and then mounted on slides for imaging. The samples were viewed at room temperature using an Olympus IX81 microscope equipped with a 100X PlanApo Oil objective (numerical aperture 1.4, $\infty/0.17$) and an ORCA-ER CCD camera (Hamamatsu Photonics) (64.5 nm effective pixel size) controlled by MetaMorph (Molecular Devices). For AF488-labeled septins, an HQ 480/40 nm excitation filter and Q 505 long-pass and HQ 535/50 nm emission filters were used (Chroma Technology Corp.). For AF555-labeled septins, an HQ 565 nm long-pass and HQ 620/60 nm emission filters (Chroma Technology Corp.) were used. Unless otherwise specified, in all micrographs the scale bar represents 10 μ m.

RESULTS

End-to-end assembly of donor- and acceptor-labeled Cdc11-capped septin hetero-octamers—Cdc11 is known to be the terminal subunit at each end of yeast septin hetero-octamers (22), which we have modeled on the basis of available crystal structures of mammalian septin complexes (37,39,40) using Phyre2 (58) (Fig. 1A). Prior work (18,22,59) has demonstrated that, in low-salt buffer, native septin hetero-octamers assemble end-on-end via formation of an NC interface between Cdc11 subunits at the ends of adjacent rods to form a long filament (Fig. 1B). During their assembly, such individual filaments pair laterally in a highly cooperative manner. This arrangement seemed highly favorable for assessing the Cdc11-Cdc11 interaction via FRET because when donor dye-labeled Cdc11-capped rods are mixed with an equimolar amount of acceptor dye-labeled Cdc11-capped rods, on average, 50% of the resulting Cdc11-Cdc11 junctions should represent donor-acceptor pairs (Fig. 1B).

We selected as the donor-acceptor dye pair AF555 and AF647, two well characterized fluorophores, quite similar to Cy3 and Cy5, a well known FRET pair (60). As required for efficient FRET, the emission of the donor (AF555) shows good spectral overlap with the absorbance of the acceptor (AF647), with only a very modest tailing into the emission of the acceptor (Fig.

1C). Moreover, according to the manufacturer (Life Technologies), the distance for 50% energy transfer (R_0) between these two dyes is 5.1 nm, and, based on our modeling, at the Cdc11-Cdc11 NC interface, dye attached to E294C in the CTE of one Cdc11 protomer should approach the dye attached to E294C in the CTE of the other Cdc11 protomer at a distance of about 3 nm.

To test these predictions, a preparation of otherwise Cys-less septin complexes containing Cdc11(E294C) was labeled with AF555 (Fig. 1D, upper) and another sample of the same complexes was labeled with AF647 (Fig. 1D, lower). Indeed, when increasing amounts of the acceptor dye-labeled rods were mixed with a fixed concentration of donor-labeled rods, and excited only at the absorbance of the donor, the characteristic spectral features of FRET were clearly observed: a diminution of the donor emission with a concomitant and corresponding increase in emission from the acceptor (Fig. 1E), as also confirmed by PCA analysis (Fig. 1E, inset). The fact that only one principal component could be detected in the FRET spectrum (unless otherwise noted, this principal component accounted for >98% of the variability in our system) indicates that the FRET observed arises from the predicted bimolecular interaction of donor dye-labeled Cdc11 and acceptor dye-labeled Cdc11 at the Cdc11-Cdc11 junctions between rods, and not from dye-dye interactions across the individual strands in paired filaments or other possible modalities, which would be expected to generate additional principal components.

Aside from revealing FRET arising from the expected close approach of donor-labeled Cdc11 and acceptor-labeled Cdc11 at the ends of the hetero-octamers, such titration experiments yield binding curves when replotted as the maximal corrected FRET observed at each of the known concentrations of acceptor dye-labeled rods that were added to the fixed known concentration of donor dye-labeled rods (Fig. 1F). Indeed, the expected approach to saturation was observed because the probability of formation of a FRET-competent Cdc11-Cdc11 junction between a donor dye-labeled rod and an acceptor dye-labeled rod should increase as the ratio of acceptor dye-labeled rods to donor dye-labeled rods increases. In addition, this very reproducible behavior indicates, contrary to

indirect experiments suggesting the opposite (61), that, once assembled, a hetero-octamer is remarkably stable, i.e. subunits in different rods do not dissociate, intermix and reassemble, at least over the time scale of our experiments. Moreover, assuming stochastic polymerization of donor- and acceptor-labeled rods, we could estimate the fraction of donor dye-labeled Cdc11-capped rods in end-to-end association with acceptor dye-labeled Cdc11-capped rods as the ratio of the concentration of the acceptor complexes divided by the total septin present (donor and acceptor complexes). In this way, such saturation curves (Fig. 1F) yield apparent K_d values for the Cdc11-Cdc11 NC interface. The average K_d^{app} value for the Cdc11-Cdc11 interaction derived from numerous experiments of this sort (Fig. 1F and 2A) was $25\text{-}30\text{ nM} \pm 11\text{ nM}$ (range) with an apparent 1:1 stoichiometry (Table 1). Furthermore, assuming an "ideal" model, namely one Cdc11 binding to one Cdc11 ($AB_{max} = 1$) and a $K_d = 25\text{ nM}$ for that interaction, generated a binding isotherm nearly identical to the observed saturation curve (Fig. 1F), fully consistent with the FRET arising purely from end-to-end assembly of donor- and acceptor-labeled Cdc11-capped septin hetero-octamers.

Linear organization of septin hetero-octamers—FRET can be used not only as a read-out for close association of a donor- and an acceptor-labeled molecule, but can also serve as a "molecular ruler" because the FRET efficiency (E) is strongly dependent on the distance between the donor and the acceptor (r), as well as on the 50% transfer distance (R_0) for the dye pair used, where F_{DA} is the fluorescence intensity of the donor with the acceptor present, and F_D is the fluorescence intensity of the donor alone (Equation 1) (62).

$$(1) \quad E = \frac{1}{\left(1 + \left(\frac{r}{R_0}\right)^6\right)} = \left(1 - \frac{F_{DA}}{F_D}\right)$$

Given the fixed order of subunits in yeast septin hetero-octamers demonstrated both *in vitro* (22) and *in vivo* (63), the observed FRET between any given donor dye-labeled septin subunit and another acceptor-dye labeled protomer should be reproducibly sensitive to its position within the rod (Fig. 2B).

Again, to test the reliability of our system to exhibit

this expected behavior, a preparation of otherwise Cys-less hetero-octamers containing Cdc11(E294C) labeled with the donor AF555 was titrated with preparations of otherwise Cys-less hetero-octamers containing respectively, Cdc11(E294C), Cdc12(L310C), Cdc3(S407C) or Cdc10(R298C) that were labeled with the acceptor AF647 (Fig. 2C). As anticipated, we observed that FRET efficiency between Cdc11-Cdc11 donor-acceptor pairs was higher than for Cdc11-Cdc12, Cdc11-Cdc3 and Cdc11-Cdc10 donor acceptor pairs. The observed FRET efficiencies were used to calculate experimentally derived distances and plotted against those values (Fig. 2D). Although no crystal structure yet exists for *S. cerevisiae* septin complexes, our homology model (Fig. 1A) and the known diameter (4 nm) of the globular GTP-binding domain of yeast septin subunits estimated from EM (22) allowed us to predict, based on end-to-end assembly, the approximated distance between the positions of the fluorophores in the different septin pairs: Cdc11-Cdc11, $\sim 2.6\text{ nm}$; Cdc11-Cdc12, $\sim 8.3\text{ nm}$; Cdc11-Cdc3, $\sim 10.8\text{ nm}$; Cdc10, $\sim 16.7\text{ nm}$. The experimentally derived values certainly follow the same trend as these predicted distances.

Especially noteworthy in this regard, however, was our finding that the calculated Cdc11-Cdc12 (5.02 nm) and Cdc11-Cdc3 (5.08 nm) distances were very similar. In the labeled Cdc12 and Cdc3 hetero-octamers, the acceptor dye is located near the base of the predicted $\alpha 6$ helix of the CTEs of these subunits, and ample evidence both *in vitro* and *in vivo* indicates that the CTEs of Cdc3 and Cdc12 are entwined in a coiled-coil interaction (22,42,59,64). Given the position at which these acceptor dyes were installed, the fact that the measured distance between the Cdc11-Cdc12 and Cdc11-Cdc3 fluorophores was so similar suggest that, relative to the donor dye in Cdc11, the acceptor dyes in Cdc12 and Cdc3 are located in very close proximity to each other. This observation is consistent with and provides additional physical evidence for the presence of an intimate coiled-coil interaction between the CTEs of Cdc12 and Cdc3. As expected, there was a marked decrease in FRET between the terminal subunit (Cdc11) and the protomer (Cdc10) situated at the greatest distance away at the center of the rod (Fig. 2D).

Although the observed FRET values displayed a clear distance sensitivity, the experimentally calculated

Novel insights about the behavior of Shs1-capped hetero-octamers—Aside from Cdc3, Cdc10, Cdc11 and Cdc12, mitotically growing yeast cells express a fifth septin, Shs1 (551 residues), that is most closely related to, but 33% larger than, Cdc11 (415 residues). Prior work has demonstrated that Shs1 can replace Cdc11 and thus serve as an alternative terminal subunit in yeast septin hetero-octamers (25). Indeed, like Cdc11-capped hetero-octamers (Fig. 4A, lower), we were able to prepare stable, otherwise Cys-less septin complexes containing Shs1(E344C) that we could efficiently label with either the donor AF555 or acceptor AF647 dyes (Fig. 4A, upper). These reagents allowed us to address several previously unresolved questions about the properties of such Shs1-capped rods.

First, EM imaging indicates that, in low-salt buffers, Shs1-capped hetero-octamers bundle and form rather thick arcs, rings, spirals and bird's nest-like arrangements (25). Given the density of these structures, it has not been possible to discern definitively whether or not Shs1-capped hetero-octamers have any capacity to join end-on-end via an Shs1-Shs1 NC interface. To address this question, a fixed concentration of donor dye-labeled Shs1(E344C)-containing rods was titrated with increasing concentrations of acceptor dye-labeled Shs1(E344C)-containing rods. Unlike the robust FRET observed for the such donor-acceptor titrations with Cdc11-capped rods (Fig. 1E), no detectable FRET occurred in the Shs1-Shs1 donor-acceptor mixtures, as evidenced by the fact that there was no internally consistent decrease in the emission of the donor and no corresponding enhancement in the emission of the acceptor above the background contribution of its increasing concentration (Fig. 4B). Thus, as judged by this criterion, Shs1-capped hetero-octamers are unable to engage in any persistent end-on-end association. Moreover, PCA of the spectral data showed two distinct principal components (Fig. 4B, inset), suggesting that the spectra recorded arise from at least two classes of weak fluorophore interactions, consistent with the complex structures formed by Shs1-capped hetero-octamers on EM grids (25). Indeed, even at the macroscopic level of the fluorescence microscope, fluorescently-tagged Shs1-capped complexes formed curved structures and even some rings (Fig. S1, left).

lengths deviated significantly from those predicted from our modeling. However, the "expected" distances were based on modeling against a rather low-resolution ($\sim 4\text{\AA}$) crystal structure of mammalian septins (39). Also, our measurements were made using pairs of donor and acceptor fluorophores located at the very end of $\alpha 6$ helix, which terminates the GTP-binding domain, at its junction with the long flexible CTE; thus, this position may have a significantly greater range of mobility than predicted. Finally, *in vivo*, septin rods assemble into filament-like structures on the cytosolic surface of the plasma membrane; however, when the septin rods assemble into filament-like structures in solution, they have a tendency to bundle laterally upon prolonged incubation or at a sufficiently high concentration (22, 44, 59). In principle, this bundling could contribute to the differences seen between the "expected" distances predicted by our modeling and the length values derived from our FRET measurements, if, for example, some filaments in such bundles were staggered (i.e. out of perfect register). Our fluorescence micrographs indicate that bundling occurs under our polymerization conditions (see Supplemental Data).

Effect of ionic strength on the Cdc11-Cdc11 NC interface—There is ample evidence that septin filaments disassemble at high ionic strength into their constituent hetero-octamers (18,20,21) and, conversely, that polymerization of Cdc11-capped hetero-octamers into long paired filaments is favored at low ionic strength (22,59). Thus, if our FRET system is reliably reporting filament assembly, the observed energy transfer between our donor dye-labeled Cdc11-capped rods and acceptor dye-labeled Cdc11-capped rods should be greatly diminished as the ionic strength is raised above the threshold required to disrupt the Cdc11-Cdc11 interaction. Indeed, when our standard titrations of donor-labeled rods with acceptor-labeled rods were conducted in buffers of increasing salt (KCl) concentration (Fig. 3A), the maximum observed FRET was progressively diminished, displaying a rather sharp transition with an EC_{50} of ~ 180 mM KCl (Fig. 3B), exhibiting an apparent Hill coefficient above 5 (Table 2), and raising the K_d^{app} from 20-30 nM to a value so weak and irreproducible ($\gg 100$ nM) that it was not possible to measure accurately (Fig. 3C).

embedded within a more continuous matrix of Cdc11-containing regions (Figs. S2A and S4A, *white arrowheads*). This organization could reflect the demonstrated capacity of Shs1-capped hetero-octamers for lateral bundling (25), such that even if an Shs1-capped rod is incorporated into these structures via its end-to-end association with Cdc11-capped rods, it could still nucleate lateral binding of additional Shs1-capped rods at the same location, resulting in the observed puncta. Presumably, the properties of such mixed assemblies give septin-based structures the flexibility and plasticity necessary to form the lattice- and gauze-like arrangements, and other supramolecular architectures, that have been observed in cells by freeze-fracture (66), cryo-electron tomography (23), and other EM methods (24).

Analysis of the role of conserved structural elements in septin-septin interaction—In the original X-ray structure of the human Sept7-Sept6-Sept2-Sept2-Sept6-Sept7 hetero-hexamers, each subunit was truncated to remove its CTE to promote crystallization (39), so no information about the disposition of those structural elements (Fig. 1A, *arrows*) was provided. Subsequently, the isolated CTEs of these same septins have been studied as purified recombinant proteins in solution, and it has been reported that the CTEs of Sept6 and Sept7 (equivalent to yeast Cdc3 and Cdc12, respectively) are able to form an elongated heterodimer with high α -helical content (presumably, a coiled coil) with a K_d of 15.8 nM (67). This value is in the same range as the Cdc11-Cdc11 and Shs1-Cdc11 interactions shown here. Moreover, although cells in which either *cdc11*(Δ CTE) or *shs1*(Δ CTE) mutants are expressed as sole source of these septins are viable, their growth and morphology are not normal (20,64). Hence, we sought to assess the contributions of the corresponding CTEs of Cdc11 and Shs1 to Cdc11-Cdc11 homotypic and Shs1-Cdc11 heterotypic association. Cdc11 and Shs1 contain CTEs that are similar, apart from a 45-residue insert (401-446) found in Shs1. Removal of the CTE (residues 306-415) from Cdc11 or of the CTE (residues 349-551) from Shs1 did not affect the engineered Cys in α 6 (E294C in Cdc11 and E344C in Shs1, respectively) that we used for maleimide labeling and do not affect the formation of stable hetero-octameric complexes

Second, it has been shown biochemically that purified Shs1 can associate with purified Cdc11 *in vitro* (20) and, as viewed in the EM, that titrating a solution of Shs1-capped hetero-octamers with increasing amounts of Cdc11-capped hetero-octamers widens the diameter and thins out the edges of the rings formed from Shs1-capped complexes, suggesting that Cdc11-capped rods can intercalate in some fashion into structures composed of Shs1-capped rods, and alter their supramolecular organization (25). These findings suggest that Cdc11-capped complexes and Shs1-capped complexes might be able to form heterotypic NC junctions. Consistent with this conclusion, we recently provided genetic evidence that such heterotypic NC junctions likely occur in the cell (65). However, there previously has been no direct and incisive means to confirm that Shs1-capped hetero-octamers are able to form heterotypic NC junctions with Cdc11-capped hetero-octamers. To test this possibility directly, we titrated several fixed concentrations of donor dye-labeled Shs1-capped rods with increasing concentrations of acceptor dye-labeled Cdc11-capped rods. In marked contrast to the Shs1-Shs1 donor-acceptor mixtures, the Shs1 donor-Cdc11 acceptor mixtures exhibited robust FRET (Fig. 4C), equivalent to that displayed by Cdc11-Cdc11 donor-acceptor mixtures (Figs. 1F and 2A). The average K_d^{app} value for the Shs1-Cdc11 interaction derived from these binding curves was ~ 20 nM \pm 10 nM (range) (Table 1), a slightly higher affinity than measured for the Cdc11-Cdc11 NC interaction. Likewise, the effect of increasing salt concentration on the stability of the Shs1-Cdc11 association displayed a somewhat broader transition and a somewhat higher EC_{50} of ~ 200 mM KCl than for the Cdc11-Cdc11 interaction (Table 2), again consistent with the Shs1-Cdc11 interaction being somewhat tighter than the Cdc11-Cdc11 interaction. Thus, we conclude that Shs1-capped hetero-octamers are indeed able to engage in a heterotypic end-on-end interaction with Cdc11-capped hetero-octamers.

Interestingly, at the macroscopic level, in 1:1 mixtures of fluorescently-tagged Shs1-capped septin complexes and Cdc11-capped septin complexes, the two dyes are clearly incorporated into the same structures (Figs. S2A and S4A); however, the Shs1-containing regions are discontinuous and appear

(25,50). Hence, we prepared, labeled and analyzed otherwise Cys-less complexes containing either Cdc11(E294C Δ CTE) or Shs1(E344C Δ CTE) (Fig. 5A). We found that absence of the CTE from Cdc11 in the acceptor dye-labeled rods, or from both the donor dye-labeled rods and the acceptor dye-labeled rods, did not have a significant effect on the FRET observed (Fig. 5B) or on the K_d^{app} value for the Cdc11-Cdc11 interaction derived from such binding curves (Table 3). Likewise, we found that removal of the CTE from Shs1 or from Cdc11, or from both, did not have a significant effect on the FRET observed (Fig. 5C) or on the K_d^{app} value for the Shs1-Cdc11 interaction derived from such binding curves (Table 3). Likewise, at the macroscopic level, fluorescently tagged hetero-octamers capped with Cdc11(Δ CTE) formed polymerized structures with either Cdc11-capped hetero-octamers or Cdc11(Δ CTE)-capped hetero-octamers with equal efficiency (Fig. S3B and C). Similarly, presence or absence of the CTE on Shs1 or Cdc11, or both, did not prevent the formation of colocalized polymerized structures closely resembling those formed between intact Shs1-capped and intact Cdc11-capped septin complexes (Fig. S2B-D). These results are consistent with our recent genetic evidence that, unlike heterodimeric coiled coil formation by the CTEs of Cdc3 and Cdc12 that contributes to the strength of their interaction (20,22,59), the CTEs of Cdc11 and Shs1 do not make a major contribution to either Cdc11-Cdc11 or Shs1-Cdc11 interaction, but rather contribute to the efficiency of recruitment *in vivo* of at least one septin-associated protein to the septin-containing structures at the bud neck (65).

Another helical element, $\alpha 0$, observed in the crystal structure of a human Sept2-Sept2 NC dimer (39), contributes some residues to the buried surface at this interface (39) and has been implicated previously in the strength of septin-septin interaction both *in vitro* (22) and *in vivo* (63). However, a tract of basic residues found within $\alpha 0$ also appears to be sufficiently surface-exposed so as to contribute to the association of septin complexes with PtdIns4,5P₂ in the plasma membrane (59,64,68). Sequence alignments and modeling indicate that all of the yeast mitotic septins have an $\alpha 0$. The apparent $\alpha 0$ in Cdc11 and Shs1 corresponds to residues 6-19 and 7-20, respectively. As analyzed by deposition onto carbon-coated grids and examination in the EM,

septin hetero-octamers capped with Cdc11(Δ 2-18), which removes essentially the entire $\alpha 0$ [hence, termed Cdc11($\Delta\alpha 0$)], were unable to polymerize in solution into filaments (22). In marked contrast, hetero-octamers capped with Cdc11($\Delta\alpha 0$) were able to assemble end-on-end to form filaments when polymerized on the surface of a PtdIns4,5P₂-containing lipid monolayer (59), indicating some significant residual capacity of the Cdc11($\Delta\alpha 0$)-capped rods to associate via the Cdc11-Cdc11 NC interface.

To explore this question further, we prepared, labeled and analyzed otherwise Cys-less complexes containing either Cdc11($\Delta\alpha 0$ E294C) or Shs1(Δ 2-18/ $\Delta\alpha 0$ E344C) (Fig. 6A). Titrating Cdc11-capped donor dye-labeled rods with Cdc11($\Delta\alpha 0$) acceptor dye-labeled rods yielded FRET behavior and an apparent affinity for Cdc11-Cdc11 interaction that was indistinguishable from that observed with wild-type Cdc11 acceptor dye-labeled rods (Fig. 6B; Table 4); however, when $\alpha 0$ was absent from the Cdc11 in both the donor dye-labeled rods and the acceptor dye-labeled rods, there was a modest, but measurable, reduction in the apparent strength of the Cdc11-Cdc11 interaction (Fig. 6B; Table 4). Similarly, when mixtures of Shs1-capped complexes and Cdc11-capped complexes were examined, the most striking effect was observed upon removal of $\alpha 0$ from Shs1 in donor dye-labeled complexes, which weakened the K_d^{app} value for the Shs1-Cdc11 interaction by 4-5 fold (Fig. 6C; Table 4); however, the noise in these particular measurements makes this value only very approximate. Nonetheless, when both Shs1 and Cdc11 lacked $\alpha 0$, interaction strength was improved (Fig. 6C; Table 4). PCA (not shown) of the same spectral data indicated maintenance of a single principal component in all these mutant combinations, supporting the view that 1:1 Cdc11-Cdc11 and Shs1-Cdc11 interactions were still able to occur *in vitro* even when these subunits lack their $\alpha 0$ element. Thus, it appears that those residues of $\alpha 0$ thought to be buried at the NC interface do not contribute in a major way to the binding energy of this interaction, at least in solution.

However, our complementary analysis of the ability of these fluorophore-labeled complexes to assemble into higher-order structures at the macroscopic level, as assessed by fluorescence microscopy, provided evidence that Cdc11 and Shs1 lacking their $\alpha 0$ are less

septin filaments at the bud neck to the yeast type II myosin (Myo1) necessary for contractile ring formation prior to cytokinesis (65,70,71).

As an initial test, we labeled purified native Bni5, which contains three endogenous Cys (C144, C266 and C375), with the acceptor dye (Fig. 7A). The efficiency with which we were able to label Bni5 with acceptor dye (2.7 AF647 molecules per protein) indicates that all three of Cys residues are solvent-exposed, consistent perhaps with structural predictions suggesting that Bni5 is a very elongated, nearly all- α -helical protein (65). Because of the multiple dyes present, we anticipated that if FRET was observed between the acceptor-labeled Bni5 and the donor dye-labeled septin filaments, any values obtained from it for apparent affinity and distance estimates would only be approximate. Nonetheless, we found that acceptor dye-labeled Bni5 showed readily detectable FRET with septin filaments containing donor dye-labelled Cdc11, and progressively lower FRET with septin filaments where the donor dye was located on another subunit (Fig. 7B), in agreement with all of the prior evidence that Bni5 associates preferentially with Cdc11 in Cdc11-capped hetero-octamers. The K_d^{app} derived for the Bni5-Cdc11 interaction from multiple titrations of donor dye-labeled Cdc11(E294C)-containing filaments was ~ 200 nM (Fig. 7C). This apparent affinity is in remarkably good agreement with a value (~ 300 nM) reported for binding of Bni5 to septin complexes measured by the technique of surface plasmon resonance (44).

DISCUSSION

FRET provides a versatile assay for monitoring septin mechanics—Prior to this work, the only assay available to observe septin assembly *in vitro* was by visual inspection of septins tagged by fusion to large genetically-encoded fluorogenic proteins under the fluorescence microscope (43). Although this technique is useful to observe the dynamics of formation of septin structures on a large scale, the protein-protein interactions intimately involved in the mechanism of septin assembly at the nanometer scale are inaccessible at the level of resolution of fluorescence microscopy. By contrast, our development of a FRET-based method enabled us to address detailed questions about the assembly mechanics and subunit interactions in septin

stable and have a tendency to mis- or unfold, as judged by the fact that the filamentous networks formed are much shorter and often contained what look like aggregates, especially when only Cdc11($\Delta\alpha 0$)-capped hetero-octamers were present (Fig. S3D and E). Similarly, in the case of mixtures of Shs1-capped complexes with Cdc11-capped complexes, removal of $\alpha 0$ from either or both of these septins altered their ability to form the higher-order structures observed with complexes capped with their wild-type counterparts. When Cdc11($\Delta\alpha 0$) complexes were combined with Shs1 complexes, there was less colocalization of Cdc11($\Delta\alpha 0$) with Shs1 and an increase in the formation of Shs1-containing puncta (Fig. S4B). Conversely, Shs1($\Delta\alpha 0$) complexes combined with Cdc11 complexes exhibited increased colocalization suggesting removal of $\alpha 0$ from Shs1 permits its more facile integration into Cdc11-containing structures (Fig. S4C). When Shs1($\Delta\alpha 0$) complexes were combined with Cdc11($\Delta\alpha 0$) complexes, however, very few organized structures of any sort were formed from either septin-containing complex (Fig. S4D). These findings could be best explained by a role for $\alpha 0$ in maintaining the stable three-dimensional fold in both Cdc11 and Shs1.

Binding and localization of a septin-associated protein—

In addition to its use in monitoring assembly of fluorophore-labeled building blocks into a polymeric structure and its utility in gauging approximate distances among fluorophore-labeled constituents of multi-protein complexes, FRET can also be used to determine whether an exogenously added, heterologous protein can associate with a pre-existing complex and the binding affinity and preferred binding site of that interaction. To test the utility of our system for this purpose, we examine the association of four derivatives of Cdc11-capped septin complexes, each donor dye-labeled on one of its component subunits and assembled into filaments at low salt concentration, with acceptor dye-labeled Bni5.

BNI5 was isolated as a dosage suppressor of *cdc12-6* and other temperature-sensitive septin mutants, and yeast two-hybrid analysis *in vivo* and GST pull-down assays *in vitro* indicated that Bni5 physically associates most strongly with Cdc11 (69). Subsequent work has demonstrated that Bni5 serves as an adaptor to link

complexes.

One major benefit of FRET is that the efficiency of the energy transfer between small, organic dye fluorophores is dependent on the distance between them in a predictable fashion and on scales relevant for septin biology. Thus, by placing FRET-compatible fluorophores on different combinations of subunits, we were able to provide independent confirmation that Cdc11-capped septin hetero-octamers assemble into filaments by end-on-end formation of homotypic Cdc11-Cdc11 junctions and not via any other sort of subunit-subunit interactions. Our measurements also provide the first quantitative estimate of the strength of the Cdc11-Cdc11 NC interface, which has a remarkably high affinity ($K_d^{app} \sim 30$ nM). Moreover, we were able to demonstrate, conversely and for the first time, that Shs1-capped hetero-octamers are incapable of engaging in end-on-end association via homotypic Shs1-Shs1 interaction. Revealingly however, and yet again for the first time, our FRET method showed that Shs1-capped hetero-octamers are capable of engaging in heterotypic Shs1-Cdc11 junctions, as had been inferred from purely circumstantial evidence based on genetic arguments in our prior studies (65). Currently, there is no evidence either *in vitro* (25) or *in vivo* (25, 63, 64, 73) that a heterooctamer can be heterotypically capped with a Cdc11 at one end and Shs1 at the other. Moreover, at a more macroscopic scale, we found that these Shs1-Cdc11 junctions are formed at a distinctly lower frequency than Cdc11-Cdc11 because Shs1-capped rods are incorporated within higher-order Cdc11-containing structures in a highly dispersed and irregularly periodic manner. This behavior is in keeping with one of the likely physiologic roles for incorporation of Shs1-capped hetero-octamers into the filaments composed of Cdc11-capped hetero-octamers, namely to assist in imparting curvature to generate and control the diameter of the septin rings at the bud neck, whose size changes during progression through the yeast cell division cycle (32,72). This hypothesis is supported by experiments in which changing the relative stoichiometry of Shs1- and Cdc11-capped hetero-octamers altered the diameter and thickness of rings observed under the EM (25), and by

the fact that, although *shs1Δ* mutants are viable, the efficiency of cytokinesis in such cells is clearly compromised (73,74).

Conditions influencing septin filament assembly—A valuable feature of our FRET-based assay, and another advantage over studies conducted using fluorescence microscopy, is that it is readily accessible to manipulation of the solvent conditions. There are many parameters that could affect septin assembly that might also be regulated in the cell, such as the guanine nucleotide concentration or pH.

Here, however, we chose to examine the effect of ionic strength because of its well-characterized influence on the state of septin filament assembly *in vitro* demonstrated in prior work (18,22). Using our FRET system, we found that the ability of Cdc11-capped rods to polymerize end-on-end into filaments is indeed salt-sensitive. The transition between filaments and isolated rods was very sharp (an apparent Hill coefficient >5) and occurred at an EC_{50} for the molarity of KCl just slightly higher (~ 180 mM) than that thought to represent the tonicity inside cells (equivalent to 120-150 mM) (75). This finding suggests that, at the ionic strength inside cells, the rod-to-filament equilibrium may be poised to be ultra-sensitive to changes in other septin effectors (*e.g.*, changes in the concentrations of particular septin subunits, GTP, and/or septin-associated proteins, or changes in post-translational modifications on septin or septin-associated proteins). If so, it would give cells the capacity to rapidly remodel septin-based structures in response to the appropriate cellular cues. Indeed, the septin cytoskeleton undergoes a variety of dramatic structural changes as the cell cycle proceeds: formation of a septin cap or nascent hoop at the incipient bud site in late G1; expansion / extension of the hoop into an hourglass-shaped collar in S to late anaphase; splitting or collapse of the collar into two bands at the onset of cytokinesis; and, breakdown of all observable higher-order septin structure prior to initiation of the next cell cycle (29,30).

In further regard to the effect of ionic strength, and given that previous observations in our own and in other laboratories have shown that septin hetero-

octamers themselves are remarkably stable even at salt concentrations as high as 300-500 mM NaCl or KCl (18,20-22), the salt-sensitive interaction responsible for salt-induced filament disassembly is clearly the Cdc11-Cdc11 NC interface. In this same regard, and given that our FRET approach was able to definitely show that Shs1-Cdc11 NC junctions are able to form robustly, and have an apparent affinity ($K_d^{app} \sim 20$ nM) even greater than Cdc11-Cdc11 junctions, it is tempting to speculate that the reported extensive and cell cycle-dependent phosphorylation of Shs1 (76,77), which does not appear to be required for Shs1 function *per se* (64), occurs as a means to enhance the efficiency of disassembly of the residual septin filaments and rings at the bud neck at the end of each cell cycle.

Analysis of conserved structural elements in septin organization—In addition to examining the properties of wild-type septin complexes, we also used our FRET methodology to explore the effect of altering certain recognized structural elements in septin monomers on the assembly properties of hetero-octamers containing them. Here, in particular, we probed the roles of the CTE and $\alpha 0$ helix in Cdc11 and in Shs1 in the formation of both homotypic Cdc11-Cdc11 interaction and in heterotypic Shs1-Cdc11 association.

Deletion of the CTE, even when removed from Cdc11 in both the donor dye-labeled Cdc11-capped complexes and the acceptor dye-labeled Cdc11 capped complexes, did not prevent formation of homotypic Cdc11-Cdc11 NC junctions or affect their apparent affinity. Likewise, deletion of the CTE from either Shs1 or Cdc11, or both, did not significantly perturb formation of heterotypic the Shs1-Cdc11 NC junction. Thus, the CTEs of Cdc11 and Shs1 do not contribute to either the Cdc11-Cdc11 or the Shs1-Cdc11 interaction, consistent with recent genetic evidence that these CTEs serve instead to enhance the recruitment of at least one septin-associated protein (65).

Our FRET system also allowed us to interrogate and answer a lingering issue about another structural element, $\alpha 0$, thought to reside at the NC interface. However, there have been conflicting views about the degree to which $\alpha 0$ is buried or solvent-exposed and

how much it contributes to the strength of the NC interaction (39,63,64). We found that removal of the $\alpha 0$ helix had no major effect on K_d^{app} for either the Cdc11-Cdc11 or the Shs1-Cdc11 interaction. Indeed, as first shown using lipid monolayers on EM grids to capture septin filament polymerization [Ref. 59], hetero-octamers capped with Cdc11($\Delta\alpha 0$) retain the capacity to assemble into filaments, in contradiction to earlier work [Ref. 22] in which similar preparations were examined for filament assembly in solution by then depositing the material on EM grids for visualizing by negative staining in the EM. Thus, our findings agree with the more recent data. It is possible that the original discrepancy arose because in the earlier study pre-formed filaments may have disassembled under the conditions required for processing of the samples, which involved solutions of heavy metals that have a high ionic strength.

Moreover, we found (see images in Supplemental Data) that, upon assembly, hetero-octamers capped with Cdc11($\Delta\alpha 0$) have a much greater tendency than hetero-octamers capped with wild-type Cdc11 to accumulate puncta and form larger-order aggregates and, in the original study, such structures (because they did not resemble long paired filaments) may have been overlooked. In any event, our findings indicate that lack of the $\alpha 0$ helix destabilizes Cdc11 and Shs1, resulting in a greater propensity for these subunits to undergo unfolding or misfolding.

Furthermore, in agreement with our FRET results indicating little direct role for the $\alpha 0$ helix in formation of the Cdc11-Cdc11 or Shs1-Cdc11 NC interfaces, there is ample evidence that the tract of basic residues in the $\alpha 0$ helix of mitotic septin subunits Cdc10 (59), Cdc11 and Shs1 (63,64) is sufficiently solvent-exposed to contribute to the interaction of septin filaments with PtdIns4,5P₂ in the plasma membrane and is required for the biological function of these septins *in vivo*. It should be conceded, that one drawback of our FRET method in solution, as it presently stands, is that it cannot assess interactions of septins with membranes or membrane surrogates.

Binding of a septin-associated protein—Finally, we demonstrated that we could apply our FRET approach to delineate the affinity of binding and the location of binding of a septin filament-associated protein. There

are a plethora of gene products that, when GFP-tagged, localize to the yeast bud neck (29,78), but in only a very few cases has it been determined which of these proteins physically associates directly with a septin or is localized at the bud neck indirectly by steric trapping or through association with the plasma membrane or with another protein that does bind directly to a septin. Our FRET method, because it uses purified components, can distinguish between these two extremes for any bud neck-localized protein that can be expressed and purified as a recombinant protein or purified to homogeneity from yeast cells.

In this regard and as a test case, we examined the association of Bni5 (Bud neck-interacting protein five) (69). We found, using our FRET assay, that Bni5 is indeed capable of binding directly to septin filaments and shows a strong preference for association with Cdc11, in agreement with results obtained by others using different *in vivo* and *in vitro* methods. Moreover, our analysis yielded a K_d^{app} value for the Bni5-Cdc11 interaction (~ 200 nM) quite similar to that (~ 300 nM) obtained by a completely different and independent biophysical method conducted by others (44). Preparing single-Cys derivatives of Bni5 will allow refinement of our binding curves to obtain more accurate assessment of its affinity and, especially, its orientation at its binding site. Furthermore, our FRET approach can be extended to defining by mutagenesis the residues in both Bni5 and Cdc11 that are essential for their high-affinity interaction.

Clearly, our system can be extended to interrogate any septin-interacting protein to determine the affinity of its binding, to pinpoint which septin subunit constitutes its preferred binding partner, and to determine its orientation relative to other landmarks in

the hetero-octamer, such as the edge from which all the CTEs project or the opposite edge (Fig. 1A). Indeed, in this regard, we have available functional single-Cys substitutions situated at various positions in and around the surface of each of the mitotic subunits (50) that could be used systematically to acquire information about such distance constraints. Similarly, with proper stopped-flow instrumentation, our FRET assay could be modified to obtain kinetic parameters for polymerization of septin hetero-octamers into filaments and to determine the rate of association of septin-binding proteins with filaments. Finally, with the proof of principle we have provided here, our FRET-based techniques could also be extended to analyze the much more complex interplay among the 13 different human septin subunits and their multifarious splice variants and other isoforms (5,79), and to address the organization and polymerization behavior of the complexes comprising them. Past work with other biopolymers, such as actin (80), have shown that the combination of spectroscopy with microscopy is exceedingly powerful for determining structure-function relationships. Relative to other cytoskeletal biopolymers, techniques for studying septins have been more rudimentary. We hope that the establishment of our FRET-based assay will provide a platform for greater understanding of how septins, their binding partners, and their regulatory factors are linked to the biological functions of these fascinating proteins.

Acknowledgements: The authors thank other members of the Thorner for their comments and suggestions during the course of these studies, Nicole Fay and Jay Groves for assistance with fluorescence microscopy, and Daniel Frank (UCSF) for his helpful insights about PCA. This work was supported by an AMGEN Scholars Summer Research Fellowship at UC Berkeley (to EWV) and by NIH R01 grants GM21841 (to JT) and GM101314 (JT and Berkeley colleague, Prof. Eva Nogales, jointly).

Conflict of Interest: The authors declare no conflicts of interest with the contents of this article.

Author Contributions: EAB and JT designed the research plan; EAB, EWV and DD devised the experimental procedures; EAB and EWV conducted the experiments and analyzed the data; EAB and JT wrote the manuscript.

REFERENCES

1. Pan, F., Malmberg, R. L., and Momany, M. (2007) Analysis of septins across kingdoms reveals orthology and new motifs. *BMC Evol. Biol.* **7**, 103.1-103.17.
2. Nishihama, R., Onishi, M., and Pringle, J. R. (2011) New insights into the phylogenetic distribution and evolutionary origins of the septins. *Biol. Chem.* **392**, 681-687.
3. McMurray, M. A., and Thorner, J. (2008) Biochemical properties and supramolecular architecture of septin hetero-oligomers and septin filaments. in "*The Septins*" (Hall, P. A., Russell, S. E. G., and Pringle, J. R. eds.), John Wiley & Sons, Ltd. , Chichester, West Sussex, UK pp 49-100.
4. Hall, P. A., and Russell, S. E. (2012) Mammalian septins: dynamic heteromers with roles in cellular morphogenesis and compartmentalization. *J. Pathol.* **226**, 287-299.
5. Fung, K. Y., Dai, L., and Trimble, W. S. (2014) Cell and molecular biology of septins. *Int. Rev. Cell Mol. Biol.* **310**, 289-339.
6. Pringle, J. R. (2008) Origins and development of the septin field. in *The Septins* (Hall, P. A., Russell, S. E. H., and Pringle, J. R. eds.), John Wiley & Sons, Ltd., Chichester, West Sussex, UK. pp 7-34.
7. Weirich, C. S., Erzberger, J. P., and Barral, Y. (2008) The septin family of GTPases: architecture and dynamics. *Nat. Rev. Mol. Cell Biol.* **9**, 478-489.
8. Hartwell, L. H. (1971) Genetic control of the cell division cycle in yeast. IV. Genes controlling bud emergence and cytokinesis. *Exp. Cell Res.* **69**, 265-276.
9. Hartwell, L. H., Culotti, J., Pringle, J. R., and Reid, B. J. (1974) Genetic control of the cell division cycle in yeast. *Science* **183**, 46-51.
10. Carroll, C. W., Altman, R., Schieltz, D., Yates, J. R., and Kellogg, D. (1998) The septins are required for the mitosis-specific activation of the Gin4 kinase. *J. Cell Biol.* **143**, 709-717.
11. Mino, A., Tanaka, K., Kamei, T., Umikawa, M., Fujiwara, T., and Takai, Y. (1998) Shs1p: a novel member of septin that interacts with spa2p, involved in polarized growth in *Saccharomyces cerevisiae*. *Biochem. Biophys. Res. Commun.* **251**, 732-736.
12. Byers, B., and Goetsch, L. (1976) A highly ordered ring of membrane-associated filaments in budding yeast. *J. Cell Biol.* **69**, 717-721.
13. Haarer, B. K., and Pringle, J. R. (1987) Immunofluorescence localization of the *Saccharomyces cerevisiae* CDC12 gene product to the vicinity of the 10-nm filaments in the mother-bud neck. *Mol. Cell. Biol.* **7**, 3678-3687.
14. Ford, S. K., and Pringle, J. R. (1991) Cellular morphogenesis in the *Saccharomyces cerevisiae* cell cycle: localization of the CDC11 gene product and the timing of events at the budding site. *Dev. Genet.* **12**, 281-292.
15. Kim, H. B., B.K., H., and Pringle, J. R. (1991) Cellular morphogenesis in the *Saccharomyces cerevisiae* cell cycle: localization of the CDC3 gene product and the timing of events at the budding site. *J. Cell Biol.* **112**, 535-544.
16. Cid, V. J., L., A., R., C., Molina, M., Sánchez, M., and Nombela, C. (1998) Cell integrity and morphogenesis in a budding yeast septin mutant. *Microbiology* **144**, 3463-3467.
17. Shulewitz, M. J., Inouye, C. J., and Thorner, J. (1999) Hsl7 localizes to a septin ring and serves as an adapter in a regulatory pathway that relieves tyrosine phosphorylation of Cdc28 protein kinase in *Saccharomyces cerevisiae*. *Mol. Cell. Biol.* **19**, 7123-7137.
18. Frazier, J. A., Wong, M. L., Longtine, M. S., Pringle, J. R., Mann, M., Mitchison, T. J., and Field, C. (1998) Polymerization of purified yeast septins: evidence that organized filament arrays may not be required for septin function. *J. Cell Biol.* **143**, 737-749.
19. Versele, M., and Thorner, J. (2004) Septin collar formation in budding yeast requires GTP binding and direct phosphorylation by the PAK, Cla4. *J. Cell Biol.* **164**, 701-715.
20. Versele, M., Gullbrand, B., Shulewitz, M. J., Cid, V. J., Bahmanyar, S., Chen, R. E., P., B., Alber, T., and Thorner, J. (2004) Protein-protein interactions governing septin heteropentamer assembly and septin filament organization in *Saccharomyces cerevisiae*. *Mol. Biol. Cell* **15**, 4568-4583.
21. Farkasovsky, M., Herter, P., Voss, B., and Wittinghofer, A. (2005) Nucleotide binding and filament assembly of recombinant yeast septin complexes. *Biol. Chem.* **386**, 643-656.

22. Bertin, A., McMurray, M.A., Grob, P., Park, S.-S., Garcia, G. III, Patanwala, I., Ng, H.-L., Alber, T., Thorner, J., Nogales, E. (2008) *Saccharomyces cerevisiae* septins: supramolecular organization of hetero-oligomers and the mechanism of filament assembly. *Proc. Natl. Acad. Sci. USA* **105**, 8274-8279.
23. Bertin, A., McMurray, M.A., Pierson, J., Thai, L., McDonald, K. L., Zehr, E.A., García, G. 3rd, Peters, P., Thorner, J., and Nogales, E. (2012) Three-dimensional ultrastructure of the septin filament network in *Saccharomyces cerevisiae*. *Mol. Biol. Cell* **23**, 423-432.
24. Ong, K., Wloka, C., Okada, S., Svitkina, T., and Bi, E. (2014) Architecture and dynamic remodelling of the septin cytoskeleton during the cell cycle. *Nat. Commun.* **5**, 5698.5691-5698.5610.
25. Garcia, G. III, Bertin, A., Li, Z., Song, Y., McMurray, M. A., Thorner, J., and Nogales, E. (2011) Subunit-dependent modulation of septin assembly: budding yeast septin Shs1 promotes ring and gauze formation. *J. Cell Biol.* **195**, 993-1004.
26. Kaplan, C., Jing, B., Winterflood, C. M., Bridges, A. a., Occhipinti, P., Schmied, J., Grinhagens, S., Gronemeyer, T., Tinnefeld, P., Gladfelter, A. S., Ries, J., and Ewers, H. (2015) The absolute arrangement of subunits in cytoskeletal septin filaments in cells measured by fluorescence microscopy. *Nano Lett.* **15**, 3859-3864.
27. Takizawa, P. A., DeRisi, J. L., Wilhelm, J. E., and Vale, R. D. (2000) Plasma membrane compartmentalization in yeast by messenger RNA transport and a septin diffusion barrier. *Science* **290**, 341-344.
28. Caudron, F., and Barral, Y. (2009) Septins and the lateral compartmentalization of eukaryotic membranes. *Dev. Cell* **16**, 493-506.
29. McMurray, M. A., and Thorner, J. (2009) Septins: molecular partitioning and the generation of cellular asymmetry. *Cell Div.* **4**, 18.1-18.14.
30. Oh, Y., and Bi, E. (2011) Septin structure and function in yeast and beyond. *Trends Cell Biol.* **21**, 141-148.
31. Tanaka-Takiguchi, Y., Kinoshita, M., and Takiguchi, K. (2009) Septin-Mediated Uniform Bracing of Phospholipid Membranes. *Curr. Biol.* **19**, 140-145.
32. Mavrikakis, M., Azou-Gros, Y., Tsai, F.C., Alvarado, J., Bertin, A., Iv, F., Kress, A., Brasselet, S., Koenderink, G., and Lecuit, T. (2014) Septins promote F-actin ring formation by crosslinking actin filaments into curved bundles. *Nat. Cell Biol.* **16**, 322-334.
33. Bridges, A.A., and Gladfelter, A. S. (2015) Septin form and function at the cell cortex. *J. Biol. Chem.* **290**, 17173-17180.
34. Kim, M. S., Froese, C. D., Estey, M. P., and Trimble, W. S. (2011) SEPT9 occupies the terminal positions in septin octamers and mediates polymerization-dependent functions in abscission. *J. Cell Biol.* **195**, 815-826.
35. Sellin, M. E., Sandblad, L., Stenmark, S., and Gullberg, M. (2011) Deciphering the rules governing assembly order of mammalian septin complexes. *Mol. Biol. Cell* **22**, 3152-3164.
36. Zent, E., Vetter, I., and Wittinghofer, A. (2011) Structural and biochemical properties of Sept7, a unique septin required for filament formation. *Biol. Chem.* **392**, 791-797.
37. Macedo, J. N., Valadares, N. F., Marques, I. A., Ferreira, F., Damalio, J. C., Pereira, H. M., Garratt, R. C., Araujo, A. P. (2013) The structure and properties of septin 3: a possible missing link in septin filament formation. *Biochem. J.* **450**, 95-105.
38. Zeraik, A. E., Pereira, H. M., Santos, Y. V., Brandão-Neto, J., Spoerner, M., Santos, M. S., Colnago, L.A., Garratt, R. C., Araújo, A.P., and DeMarco, R. (2014) Crystal structure of a *Schistosoma mansoni* septin reveals the phenomenon of strand slippage in septins dependent on the nature of the bound nucleotide. *J. Biol. Chem.* **289**, 7799-7811.
39. Sirajuddin, M., Farkasovsky, M., Hauer, F., Kühlmann, D., Macara, I. G., Weyand, M., Stark, H., and Wittinghofer, A. (2007) Structural insight into filament formation by mammalian septins. *Nature* **449**, 311-315.
40. Sirajuddin, M., Farkasovsky, M., Zent, E., and Wittinghofer, A. (2009) GTP-induced conformational changes in septins and implications for function. *Proc. Natl. Acad. Sci. USA* **106**, 16592-16597.
41. Zent, E., and Wittinghofer, A. (2014) Human septin isoforms and the GDP-GTP cycle. *Biol. Chem.* **395**, 169-180.
42. Barth, P., Schoeffler, A., and Alber, T. (2008) Targeting metastable coiled-coil domains by computational design. *J. Am. Chem. Soc.* **130**, 12038-12044.
43. Bridges, A. A., Zhang, H., Mehta, S. B., Occhipinti, P., Tani, T., and Gladfelter, A. S. (2014) Septin assemblies form

- by diffusion-driven annealing on membranes. *Proc. Natl. Acad. Sci. USA* **111**, 2146-2151.
44. Renz, C., Johnsson, N., and Gronemeyer, T. (2013) An efficient protocol for the purification and labeling of entire yeast septin rods from E.coli for quantitative in vitro experimentation. *BMC Biotechnol.* **13**, 60.1-60.8.
 45. Bonne, D., Heusele, C., Simon, C., and Pantaloni, D. (1985) 4',6-Diamidino-2-phenylindole, a fluorescent probe for tubulin and microtubules. *J. Biol. Chem.* **280**, 2819-2825.
 46. Sackett, D. L., Knutson, J. R., and Wolff, J. (1990) Hydrophobic surfaces of tubulin probed by time-resolved and steady-state fluorescence of Nile red. *J. Biol. Chem.* **265**, 14899-14906.
 47. Cooper, J.A., Walker, S.B., and Pollard, T.D. (1983) Pyrene actin: documentation of the validity of a sensitive assay for actin polymerization. *J. Muscle Res. Cell Motil.* **4**, 253-262.
 48. Hansen, S. D., Zuchero, J. B., and Mullins, R. D. (2013) Cytoplasmic actin: Purification and single molecule assembly assays. *Methods Mol. Biol.* **1046**, 145-170.
 49. Bolanos-Garcia, V. M., and Davies, O. R. (2006) Structural analysis and classification of native proteins from E. coli commonly co-purified by immobilised metal affinity chromatography. *Biochim. Biophys. Acta* **1760**, 1304-1313.
 50. de Val, N., McMurray, M. A., Lam, L. H., Hsiung, C. C., Bertin, A., Nogales, E., and Thorner, J. (2013) Native cysteine residues are dispensable for the structure and function of all five yeast mitotic septins. *Proteins* **81**, 1964-1979.
 51. Wang, W., and Malcolm, B. A. (1999) Two-stage PCR protocol allowing introduction of multiple mutations, deletions and insertions using Quik-Change™ site-directed mutagenesis. *Biotechniques* **26**, 680-682.
 52. Li, M. Z., and Elledge, S. J. (2012) SLIC: a method for sequence- and ligation-independent cloning. *Methods Mol. Biol.* **852**, 51-59.
 53. Smith, P. K., Krohn, R. I., Hermanson, G. T., Mallia, a. K., Gartner, F. H., Provenzano, M. D., Fujimoto, E. K., Goeke, N. M., Olson, B. J., and Klenk, D. C. (1985) Measurement of protein using bicinchoninic acid. *Anal. Biochem.* **150**, 76-85.
 54. Al-Soufi, W., Novo, M., Mosquera, M., and Rodríguez-Prieto, F. (2009) Principal component global analysis of series of fluorescence spectra. in *Reviews in Fluorescence* (Geddes, C.D., ed.), Springer Science, pp 23-45.
 55. Song, Y., Madahar, V., and Liao, J. (2011) Development of FRET assay into quantitative and high-throughput screening technology platforms for protein-protein interactions. *Ann. Biomed. Eng.* **39**, 1224-1234.
 56. Hieb, A. R., D'Arcy, S., Kramer, M. a., White, A. E., and Luger, K. (2012) Fluorescence strategies for high-throughput quantification of protein interactions. *Nucleic Acids Res.* **40**, e33.1-e33.13.
 57. Zeug, A., Woehler, A., Neher, E., and Ponimaskin, E. G. (2012) Quantitative intensity-based FRET approaches - A comparative snapshot. *Biophys. J.* **103**, 1821-1827.
 58. Kelley, L.A., Mezulis, S., Yates, C. M., Wass, M. N., and Sternberg, M. J. E. (2015) The Phyre2 web portal for protein modeling, prediction and analysis. *Nat. Protoc.* **10**, 845-858.
 59. Bertin, A., McMurray, M.A., Thai, L., Garcia, G. III, Votin, V., Grob, P., Allyn, T., Thorner, J., and Nogales, E. (2010) Phosphatidylinositol-4,5-bisphosphate promotes budding yeast septin filament assembly and organization. *J. Mol. Biol.* **404**, 711-731.
 60. Kenworthy, A. K. (2001) Imaging protein-protein interactions using fluorescence resonance energy transfer microscopy. *Methods* **24**, 289-296.
 61. McMurray, M. A., and Thorner, J. (2008) Septin stability and recycling during dynamic structural transitions in cell division and development. *Curr. Biol.* **18**, 1203-1208.
 62. Lakowicz, J. R. (2006) *Principles of Fluorescence Spectroscopy, 3rd Ed.*, Springer Science, 953 pp.
 63. McMurray, M. A., Bertin, A., Garcia, G., 3rd, Lam, L., Nogales, E., and Thorner, J. (2011) Septin filament formation is essential in budding yeast. *Dev. Cell* **20**, 540-549.
 64. Finnigan, G. C., Takagi, J., Cho, C., and Thorner, J. (2015) Comprehensive genetic analysis of paralogous terminal septin subunits Shs1 and Cdc11 in *Saccharomyces cerevisiae*. *Genetics* **200**, 821-841.
 65. Finnigan, G. C., Booth, E. A., Duvalyan, A., Liao, E. N., and Thorner, J. (2015) The carboxy-terminal tails of septins Cdc11 and Shs1 recruit myosin-II binding factor Bni5 to the bud neck in *Saccharomyces cerevisiae*. *Genetics* **200**, 843-862.

66. Rodal, A. A., Kozubowski, L., Goode, B. L., Drubin, D. G., and Hartwig, J. H. (2005) Actin and septin ultrastructures at the budding yeast cell cortex. *Mol. Biol. Cell* **16**, 372-384.
67. de Almeida Marques, I., Valadares, N. F., Garcia, W., Damalio, J. C., Macedo, J. N., de Araújo, A. P., Botello, C. A., Andreu, J. M., and Garratt, R. C. (2012) Septin C-terminal domain interactions: implications for filament stability and assembly. *Cell Biochem. Biophys.* **62**, 317-328.
68. Zhang, J., Kong, C., Xie, H., McPherson, P. S., Grinstein, S., and Trimble, W. S. (1999) Phosphatidylinositol polyphosphate binding to the mammalian septin H5 is modulated by GTP. *Curr. Biol.* **9**, 1458-1467.
69. Lee, P. R., Song, S., Ro, H. S., Park, C. J., Lippincott, J., Li, R., Pringle, J. R., De Virgilio, C., Longtine, M. S., and Lee, K. S. (2002) Bni5p, a septin-interacting protein, is required for normal septin function and cytokinesis in *Saccharomyces cerevisiae*. *Mol. Cell. Biol.* **22**, 6906-6920.
70. Fang, X., Luo, J., Nishihama, R., Wloka, C., Dravis, C., Travaglia, M., Iwase, M., Vallen, E. A., and Bi, E. (2010) Biphasic targeting and cleavage furrow ingression directed by the tail of a myosin II. *J. Cell Biol.* **191**, 1333-1350.
71. Schneider, C., Grois, J., Renz, C., Gronemeyer, T., and Johnsson, N. (2013) Septin rings act as a template for myosin higher-order structures and inhibit redundant polarity establishment. *J. Cell Sci.* **126**, 3390-3400.
72. Ong, K., Wloka, C., Okada, S., Svitkina, T., and Bi, E. (2014) Architecture and dynamic remodelling of the septin cytoskeleton during the cell cycle. *Nat. Commun.* **81**, 8715-8723.
73. Iwase, M., Luo, J., Bi, E., and Toh-e, A. (2007) Shs1 plays separable roles in septin organization and cytokinesis in *Saccharomyces cerevisiae*. *Genetics* **177**, 215-229.
74. BATTERY, S. M., KONO, K., STOKASIMOV, E., and PELLMAN, D. (2012) Regulation of the formin Bnr1 by septins and a MARK/Par1-family septin-associated kinase. *Mol. Biol. Cell* **23**, 4041-4053.
75. Miller, D. J. (2004) Sydney Ringer; physiological saline, calcium and the contraction of the heart. *J. Physiol.* **555**, 585-587.
76. Dobbelaere, J., Gentry, M. S., Hallberg, R. L., and Barral, Y. (2003) Phosphorylation-dependent regulation of septin dynamics during the cell cycle. *Dev. Cell* **4**, 345-357.
77. Egelhofer, T. A., Villen, J., McCusker, D., Gygi, S. P., and Kellogg, D. R. (2008) The septins function in G1 pathways that influence the pattern of cell growth in budding yeast. *PLoS One* **3**, e2022.2021-e2022.2014.
78. Gladfelter, A. S., Pringle, J. R., and Lew, D. J. (2001) The septin cortex at the yeast mother-bud neck. *Curr. Opin. Microbiol.* **4**, 681-689.
79. Spiliotis, E. T., and Nelson, W. J. (2006) Here come the septins: novel polymers that coordinate intracellular functions and organization. *J. Cell Sci.* **119**, 4-10.
80. Pollard, T. D., and Cooper, J. A. (2009) Actin, a central player in cell shape and movement. *Science* **326**, 1208-1212.

FOOTNOTES

^aCurrent Address: Grifols Diagnostic Solutions Inc., 4560 Horton St, Emeryville, CA 94608

^bCurrent Address: Dept. of Medicinal Chemistry, School of Pharmacy, Univ. of Washington, Seattle, WA 98195

^cCurrent Address: Novartis Institutes for BioMedical Research, 5300 Chiron Way, Emeryville, CA 94608

³Abbreviations used: Alexa Fluor 488 maleimide (AF488), Alexa Fluor 555 maleimide (AF555), Alexa Fluor 647 maleimide (AF647), apparent dissociation constant (K_d^{app}), C-terminal extension (CTE), dithiothreitol (DTT), electron microscopy (EM), fast protein liquid chromatography (FPLC), Förster resonance energy transfer (FRET), immobilized metal ion affinity chromatography (IMAC), nitrilotriacetate (NTA), open reading frame (ORF), principal component analysis (PCA), poly-L-lysine (PLL), phosphatidylinositol 4,5-bisphosphate (PtdIns4,5P₂), tris-(2-carboxyethyl)phosphine (TCEP).

Figure Legends

Figure 1: Labeling terminal septin subunit (Cdc11) allows for establishment of a FRET system. (A) Schematic representation of subunits within the yeast septin octamer as predicted by Phyre II and aligned to the crystal structure of the human septin hexamer (2QAG) in Pymol. (B) Schematic showing possible arrangements of Cdc11 labeled septin subunits. Donor and acceptor labeled septins are allowed to assemble stochastically. (C) Normalized excitation and emission spectra as measured of AF555 and AF647. (D) Coomassie gels and typhoon scans of Cdc11 septin octamers labeled at the terminal septin with AF555 and AF647. (E) FRET emission spectra with 25 nM Cdc11^{AF555} labeled octamers recorded at increasing concentrations of Cdc11^{AF647} labeled octamers: 0.78 nM, dashed green; 1.56 nM, dashed cyan; 3.13 nM, dashed red; 6.25 nM, dashed black; 12.5 nM, solid green; 25 nM, solid cyan; 50 nM, solid red; and, 100 nM, solid black. Inset illustrates the result of the PCA. (F) Binding curve corresponding to fluorescence spectra in E. Black circles with SEM error bars correspond to experimental data. Black line shows the fitted binding curve. Red curve is the predicted binding curve from stochastic assembly of the septin polymeric complex.

Figure 2: FRET is sensitive to subunit labeling. (A) Binding curves for Cdc11 AF555 and Cdc11 AF647 using varying concentrations of Cdc11^{AF555} (25 nM Cdc11^{AF555} (red), 35 nM Cdc11^{AF555} (cyan), 50 nM Cdc11^{AF555} (magenta)). (B) Schematic showing labeling of septin octamer at different subunits. The Cdc11^{AF555} is kept constant while the acceptor (AF647) is transferred along the septin octamer. This schematic corresponds to the results in (C & D). (C) Coomassie gels and typhoon scans of labeled septin octamers with AF555 and AF647. (D) Red curve shows the predicted efficiency of transfer from the FRET equation. Black circles with SEM error bars correspond to experimental data for a 1:4 mixture of Cdc11^{AF555}:acceptor labeled septin. The data points are labeled for the labeled septins (Donor-Acceptor) in the FRET system.

Figure 3: Effect of ionic strength on septin assembly. (A) A series of binding curves for Cdc11 labeled septin subunits assembled under varying ionic strength using the FRET corrected method. (B) Using PCA and 1:1 mixture of Cdc11^{AF555}:Cdc11^{AF647}, apparent Hill coefficients and EC₅₀ can be determined as a function of ionic strength. The light gray line illustrates the location of the EC₅₀ value. (C) Bar graphs illustrate the values of binding constants corresponding to the color matched curves in (A).

Figure 4: Labeling of alternate terminal septin subunit (Shs1) does not establish a FRET system without Cdc11. (A) Coomassie gels and typhoon scans of labeled septin octamers with AF555 and AF647 using end subunits of Shs1 and Cdc11. (B) FRET emission spectra with 25 nM Shs1^{AF555} labeled octamers recorded at increasing concentrations of Shs1^{AF647} labeled octamers: 0.78 nM, dashed green; 1.56 nM, dashed cyan; 3.13 nM, dashed red; 6.25 nM, dashed black; 12.5 nM, solid green; 25 nM, solid cyan; 50 nM, solid red; and, 100 nM, solid black. Inset illustrates the result of the PCA with at least 2 principal components. (C) Binding curves of Cdc11^{AF647} capped octamers with Shs1^{AF555} capped octamers at varying concentration of Shs1^{AF555}. (25 nM Shs1^{AF555} (red), 35 nM Shs1^{AF555} (cyan), 50 nM Shs1^{AF555} (magenta)) (D) Using PCA, Hill coefficients and IC₅₀ can be determined as a function of ionic strength. The light red line illustrates the location of the IC₅₀ value. The Cdc11^{AF555}-Cdc11^{AF647} (black line) is included for reference.

Figure 5: Affect of deletion of the terminal subunit C-terminal extension on septin octamer assembly by FRET. (A) Coomassie gels and typhoon scans of labeled septin octamers with AF555 and AF647 using end subunits of Shs1 ΔCTE and Cdc11 ΔCTE. (B) Binding curves for Cdc11^{AF555} - Cdc11^{AF647} (red), Cdc11^{AF555} - Cdc11 ΔCTE^{AF647} (cyan), and Cdc11 ΔCTE^{AF555} - Cdc11 ΔCTE^{AF647} (magenta). (C) Binding curves for Shs1^{AF555} - Cdc11^{AF647} (red), Shs1^{AF555} - Cdc11 ΔCTE^{AF647} (cyan), Shs1 ΔCTE^{AF555} - Cdc11^{AF647} (magenta), Shs1 ΔCTE^{AF555} - Cdc11 ΔCTE^{AF647} (black). For (B & C) dots represents measured data and color coded lines the corresponding binding curve fit.

Figure 6: Affect of deletion of the terminal subunit α0 helix on septin octamer assembly by FRET. (A) Coomassie gels and typhoon scans of labeled septin octamers with AF555 and AF647 using end subunits of Shs1 Δα0 and Cdc11 Δα0. (B)

Binding curves for Cdc11^{AF555} – Cdc11^{AF647} (red), Cdc11^{AF555} – Cdc11 $\Delta\alpha0$ ^{AF647} (cyan), and Cdc11 $\Delta\alpha0$ ^{AF555} – Cdc11 $\Delta\alpha0$ ^{AF647} (magenta). (C) Binding curves for Shs1^{AF555} – Cdc11^{AF647} (red), Shs1^{AF555} – Cdc11 $\Delta\alpha0$ ^{AF647} (cyan), Shs1 $\Delta\alpha0$ ^{AF555} – Cdc11^{AF647} (magenta), Shs1 $\Delta\alpha0$ ^{AF555} – Cdc11 $\Delta\alpha0$ ^{AF647} (black). For (B & C) dots represents measured data and color coded lines the corresponding binding curve fit.

Figure 7: Bni5 binding to septin hetero-octamers. A) Coomassie gel and typhoon scan of Bni5 purified and labeled with AF647 including position of ladder. B) Bar graph showing the measured efficiency of transfer for acceptor dye-labeled Bni5 with each donor-dye labeled septin subunit in Cdc11-capped hetero-octamers. ANOVA ($p < 0.05$) show significant increase in efficiency of transfer between Bni5 with Cdc11 over Cdc3 and Cdc10 labeled subunits. C) Binding curves of Bni5^{AF647} (max 500 nM) with Cdc11^{AF555} (15 nM (dashed line), 25 nM (solid line)) septin octamers with measured K_d values of 221.5 ± 148.5 nM and 210.2 ± 99.9 nM respectively (mean \pm values show the confidence interval calculated for $p = 0.05$).

Table 1: Parameters from analysis of septin assembly with varying concentrations.

Each value in the table represents the average of measurements made in triplicate and the \pm values show the confidence interval calculated for $p = 0.05$.

FRET Pair (Donor – Acceptor)	Donor Conc. [nM]	Apparent K_d [nM]	Apparent AB_{max} (fraction donor in FRET)
Cdc11 ^{AF555} -Cdc11 ^{AF647}	25	20.19 \pm 18.97	0.97 \pm 0.26
Cdc11 ^{AF555} -Cdc11 ^{AF647}	35	34.52 \pm 34.87	1.20 \pm 0.43
Cdc11 ^{AF555} -Cdc11 ^{AF647}	50	38.77 \pm 27.72	1.28 \pm 0.34
Shs1 ^{AF555} -Cdc11 ^{AF647}	25	10.78 \pm 8.08	0.79 \pm 0.15
Shs1 ^{AF555} -Cdc11 ^{AF647}	35	21.26 \pm 28.72	0.90 \pm 0.36
Shs1 ^{AF555} -Cdc11 ^{AF647}	50	27.51 \pm 21.25	1.09 \pm 0.27

Table 2: Parameter from the analysis of septin assembly as a function of ionic strength.

Each value in the table represents the average of measurements made in triplicate and the \pm values show the confidence interval calculated for $p = 0.05$. Equimolar quantities of donor and acceptor were present while varying ionic strength.

FRET Pair (Donor – Acceptor)	Ionic Strength at EC_{50} [mM]	Apparent Hill Coefficient
Cdc11 ^{AF555} -Cdc11 ^{AF647}	181.20 \pm 46.50	5.50 \pm 6.25
Shs1 ^{AF555} -Cdc11 ^{AF647}	197.90 \pm 40.40	2.68 \pm 1.39

Table 3: Parameters for the analysis of septin assembly with Δ CTE septins.

Each value in the table represents the average of measurements made in triplicate and the \pm values show the confidence interval calculated for $p = 0.05$. The donor was held at 25 nM and FRET was measured in the absence and presence of increasing concentrations of acceptor up to 100 nM.

FRET Pair (Donor – Acceptor)	Apparent K_d [nM]	Apparent AB_{max} (fraction donor in FRET)
Cdc11 ^{AF555} -Cdc11 Δ CTE ^{AF647}	24.11 \pm 11.45	1.15 \pm 0.17
Cdc11 Δ CTE ^{AF555} -Cdc11 Δ CTE ^{AF647}	17.68 \pm 17.65	0.88 \pm 0.24
Shs1 ^{AF555} -Cdc11 Δ CTE ^{AF647}	22.24 \pm 16.45	1.06 \pm 0.23
Shs1 Δ CTE ^{AF555} -Cdc11 ^{AF647}	30.38 \pm 12.83	1.17 \pm 0.17
Shs1 Δ CTE ^{AF555} -Cdc11 Δ CTE ^{AF647}	22.83 \pm 7.95	1.13 \pm 0.12

Table 4: Parameters for the analysis of septin assembly with $\Delta\alpha 0$ septins.

Each value in the table represents the average of measurements made in triplicate and the \pm values show the confidence interval calculated for $p = 0.05$. The donor was held at 25 nM and FRET was measured in the absence and presence of increasing concentrations of acceptor up to 100 nM.

FRET Pair (Donor – Acceptor)	Apparent K_d [nM]	Apparent AB_{max} (fraction donor in FRET)
Cdc11 ^{AF555} -Cdc11 $\Delta\alpha 0$ ^{AF647}	19.49 \pm 8.23	1.00 \pm 0.12
Cdc11 $\Delta\alpha 0$ ^{AF555} -Cdc11 $\Delta\alpha 0$ ^{AF647}	33.21 \pm 19.17	1.07 \pm 0.22
Shs1 ^{AF555} -Cdc11 $\Delta\alpha 0$ ^{AF647}	8.13 \pm 4.47	0.75 \pm 0.10
Shs1 $\Delta\alpha 0$ ^{AF555} -Cdc11 ^{AF647}	40.58 \pm 58.31	1.28 \pm 0.61
Shs1 $\Delta\alpha 0$ ^{AF555} -Cdc11 $\Delta\alpha 0$ ^{AF647}	9.89 \pm 8.93	0.80 \pm 0.18

Figure 1

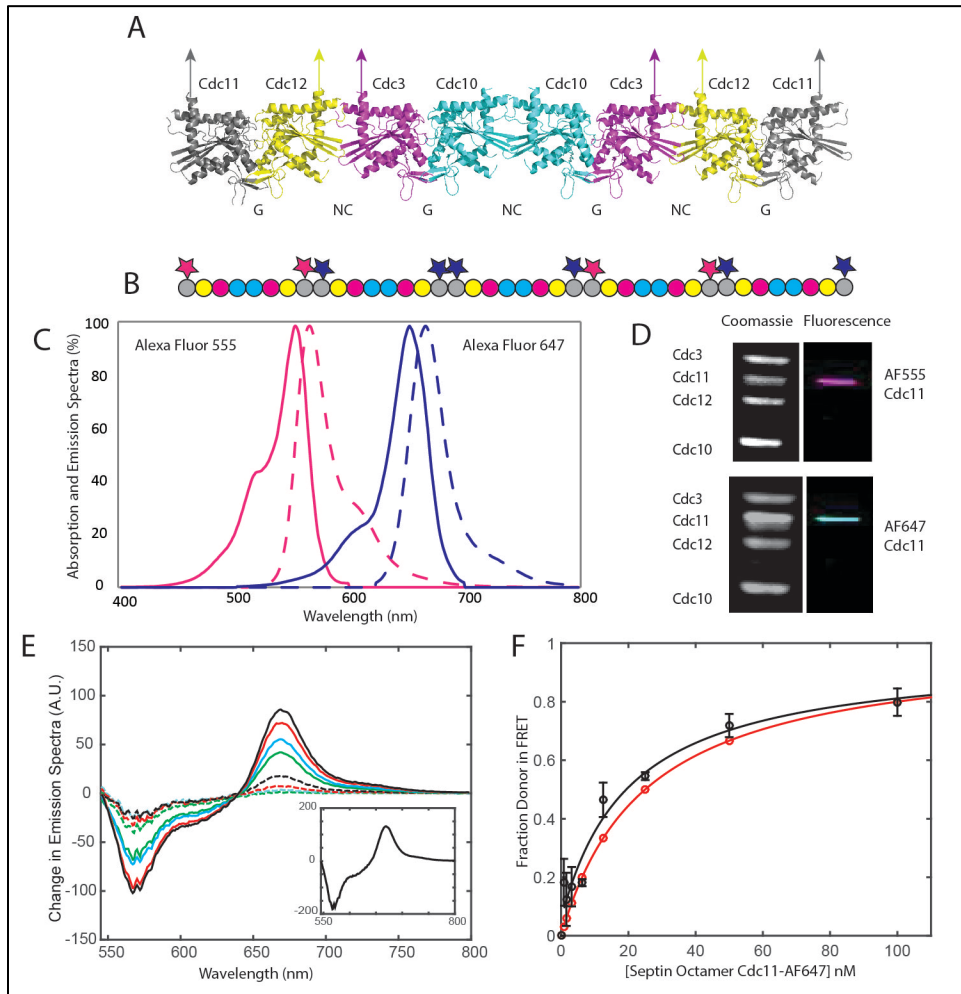


Figure 2

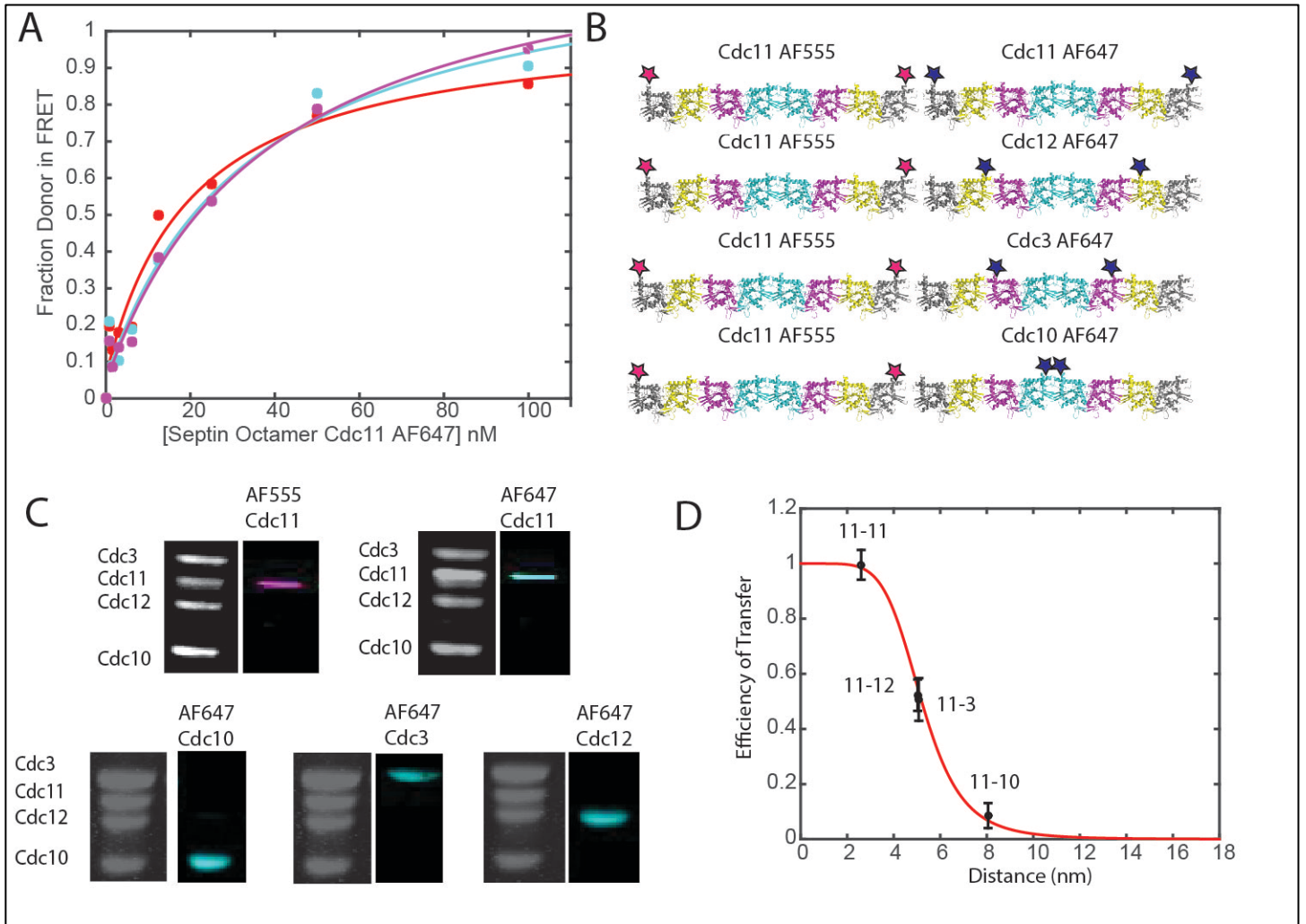


Figure 3

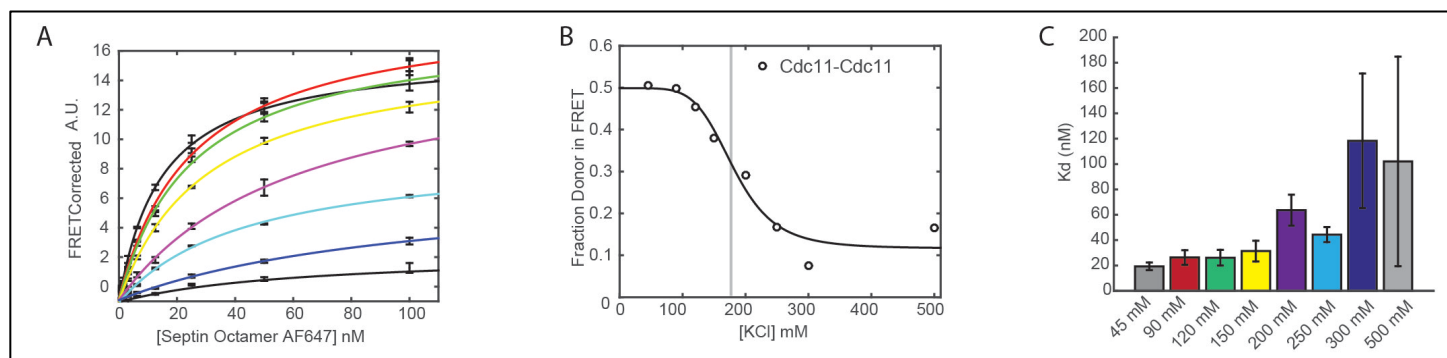


Figure 4

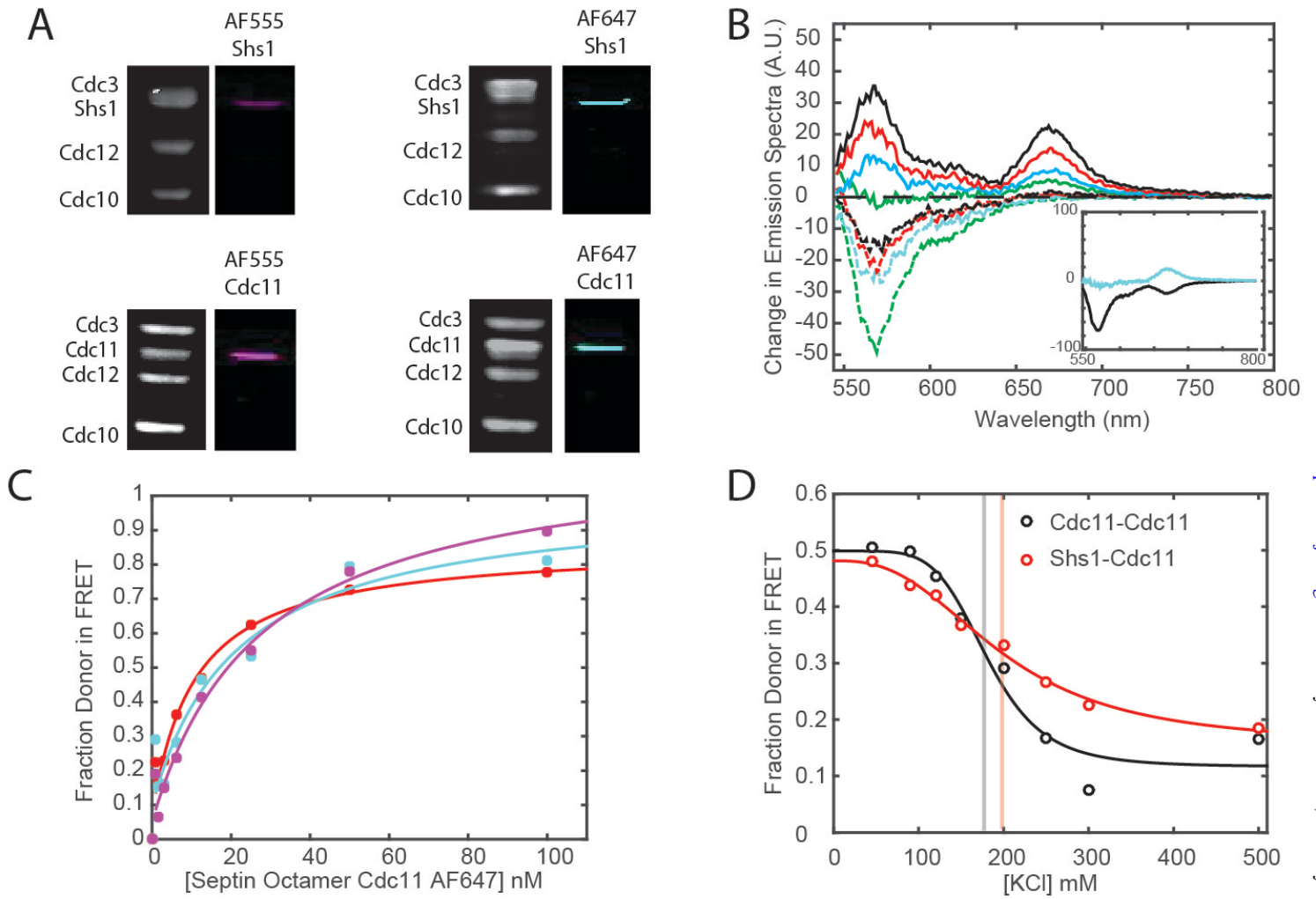


Figure 5

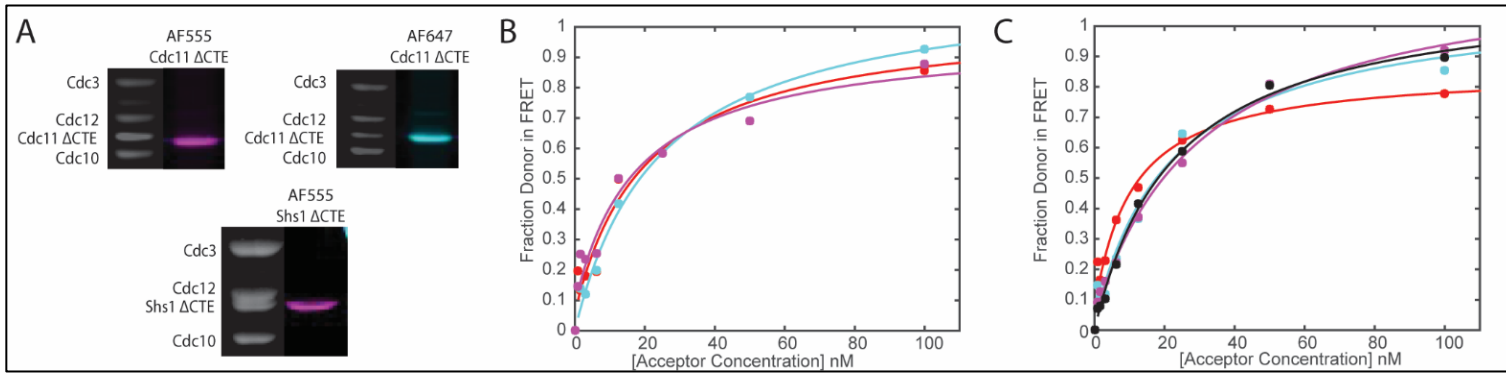


Figure 6

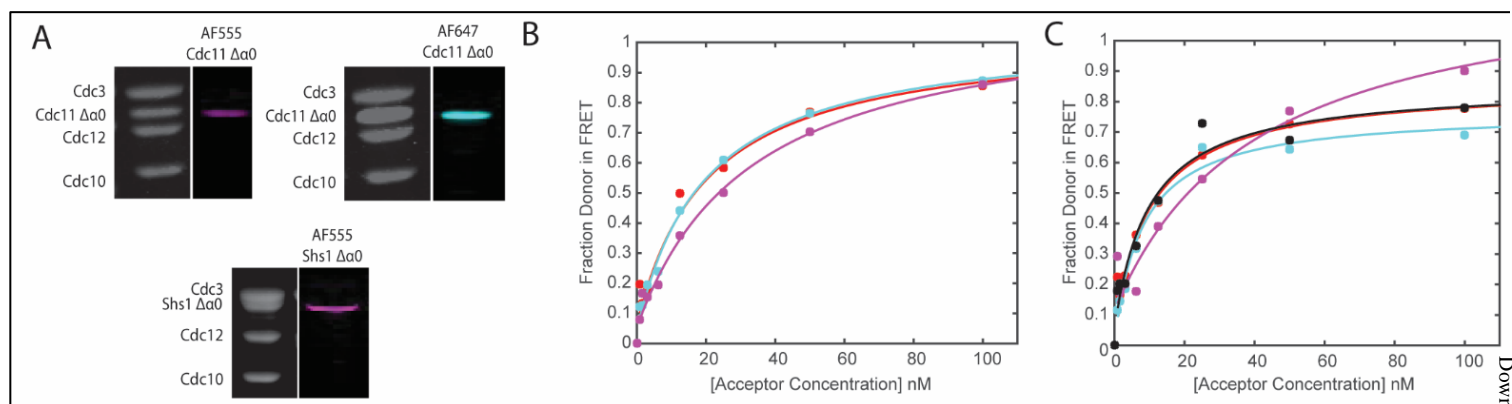
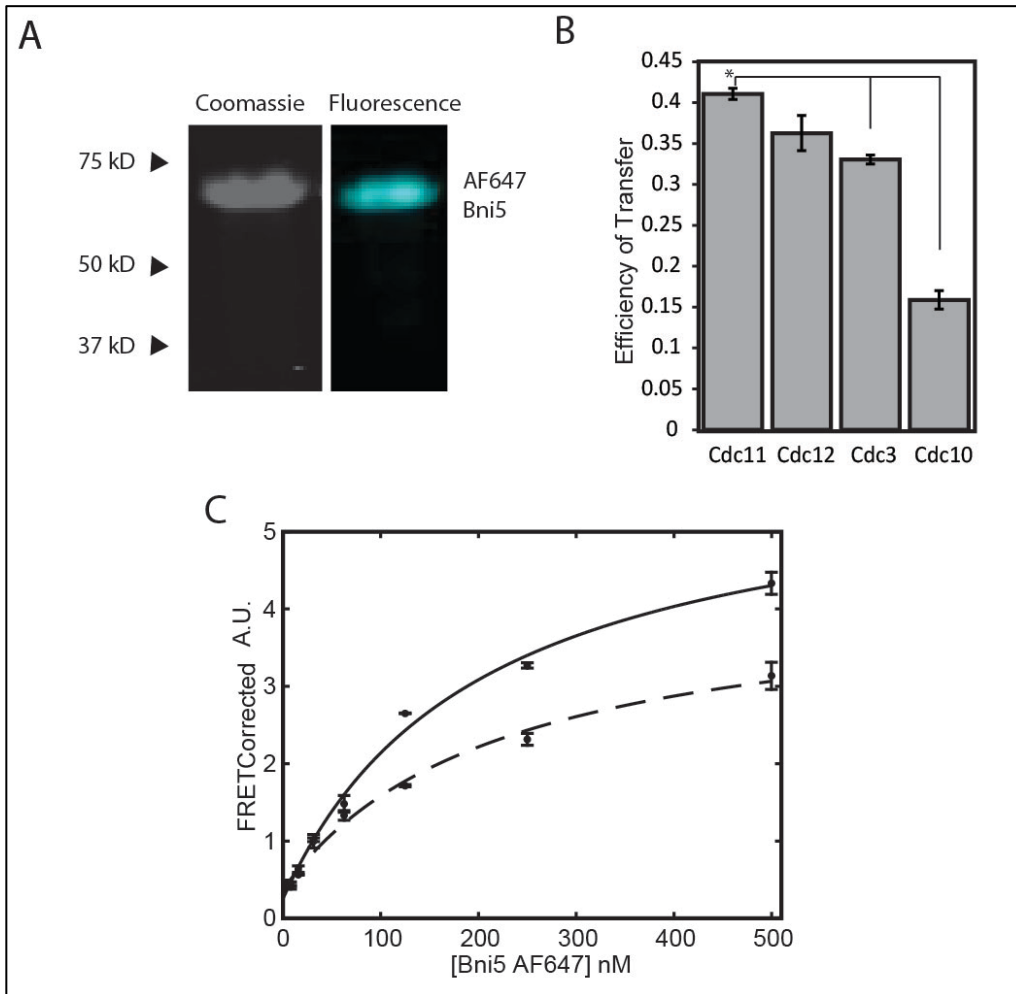


Figure 7



SUPPLEMENTAL INFORMATION

A FRET-based System Provides Insight into the Ordered Assembly of Yeast Septin Hetero-octamers

Elizabeth A. Booth^{1a}, Eleanor W. Vane^{1b}, Dustin Dovala^{2c} and Jeremy Thorner^{1*}

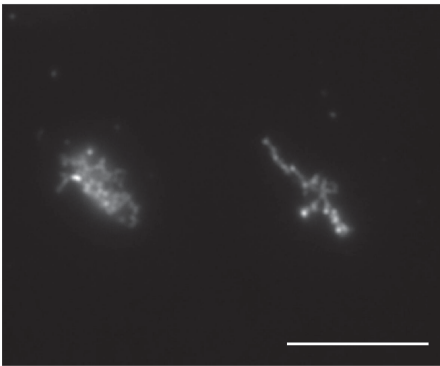
¹Division of Biochemistry, Biophysics, and Structural Biology, Department of Molecular and Cell Biology, University of California, Berkeley, CA 94720-3202

²Program in Microbial Pathogenesis and Host Defense, Department of Microbiology and Immunology, University of California School of Medicine, San Francisco, CA 94158-2200

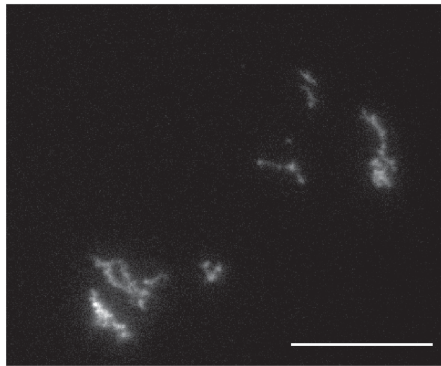
Running title: *A spectroscopic approach for analysis of septin assembly*

*To whom correspondence should be addressed: Prof. Jeremy Thorner, Dept. of Molecular and Cell Biology, University of California, Rm. 526, Barker Hall, Berkeley, CA 94720-3202. Phone: (510) 642-2558, FAX: (510) 642- 6420, E-mail: jthorner@berkeley.edu

Shs1 AF555



Shs1 ΔCTE AF555



Shs1 Δα0 AF555

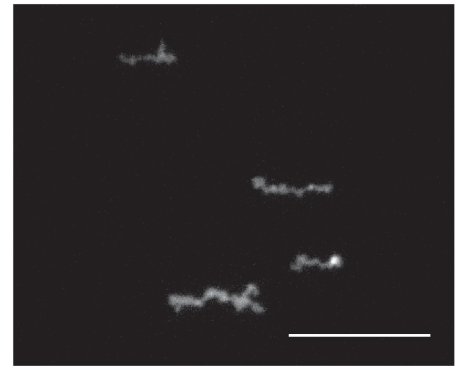


Figure S1: Micrographs of assembled Shs1 septins. Shs1^{AF555} constructs self-assembled for 1 hour at room temperature before plating on PLL coated slides.

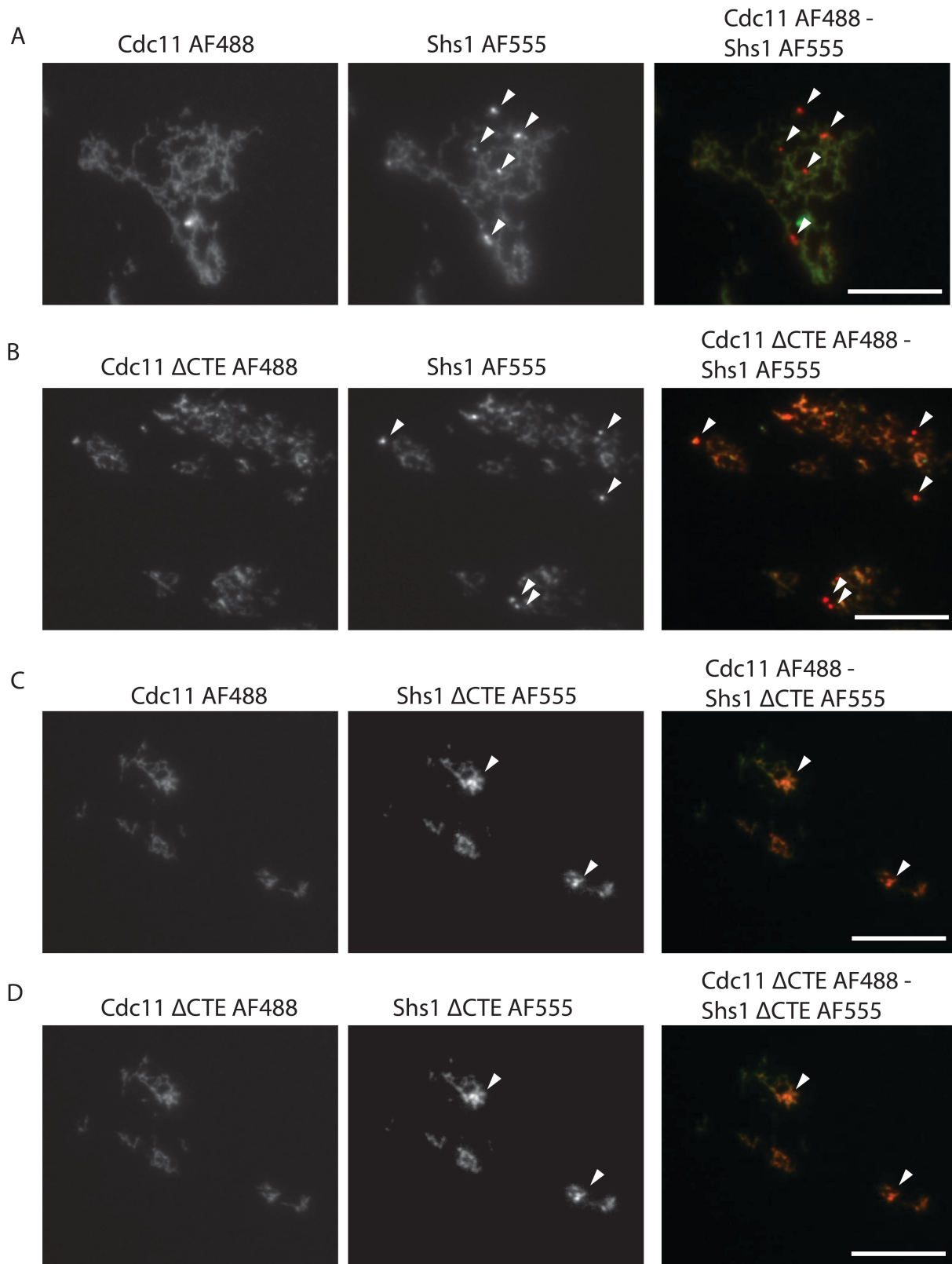


Figure S2: Micrographs of assembled Cdc11 and Shs1 septins with CTE deletions. Equimolar concentrations for Cdc11^{AF488} septins and Shs1^{AF555} septins self-assembled for 1 hour at room temperature before plating on PLL coated slides. (A-D) Leftmost column shows the Cdc11^{AF488} construct. The center column shows the Shs1^{AF555} construct. The rightmost column shows the overlay of the AF555 and AF488 labeled constructs. Arrows indicate the formation of Shs1 puncta.

A spectroscopic approach for analysis of septin assembly

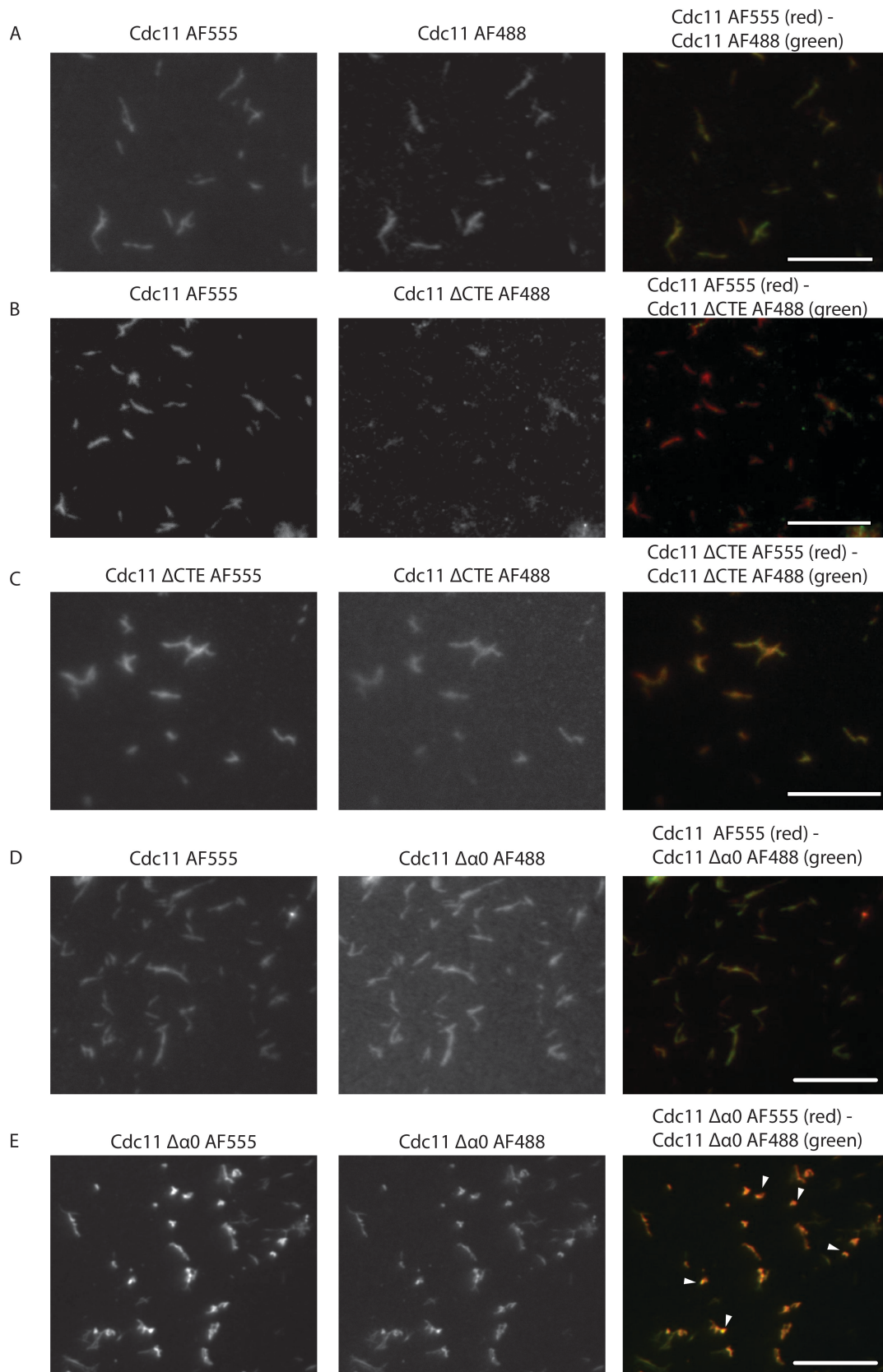


Figure S3: Micrographs of assembled Cdc11 septins. Equimolar concentrations for AF488 and AF555 labeled septins self-assembled for 1 hour at room temperature before plating on PLL coated slides. (A-E) Leftmost column shows the Cdc11^{AF555} construct. The center column shows the Cdc11^{AF488} construct. The rightmost column shows the overlay of the AF555 and AF488 labeled constructs.

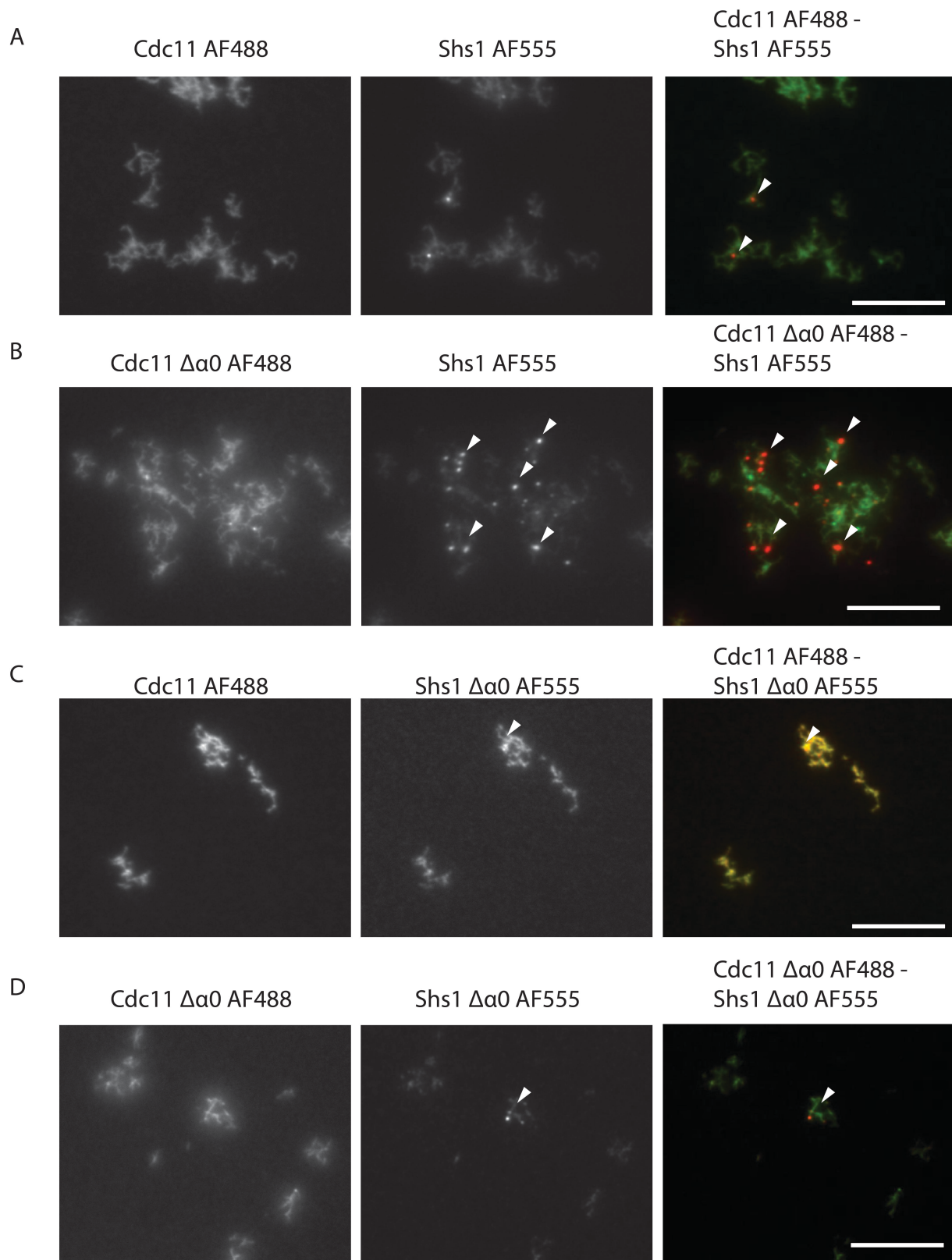


Figure S4: Micrographs of assembled Cdc11 and Shs1 septins with $\alpha 0$ deletions. Equimolar concentrations for Cdc11^{AF488} septins and Shs1^{AF555} septins self-assembled for 1 hour at room temperature before plating on PLL coated slides. (A-D) Leftmost column shows the Cdc11^{AF488} construct. The center column shows the Shs1^{AF555} construct. The rightmost column shows the overlay of the AF555 and AF488 labeled constructs. Arrows indicate the formation of Shs1 puncta.

Cell Biology:

A Foerster Resonance Energy Transfer (FRET)-based System Provides Insight into the Ordered Assembly of Yeast Septin Hetero-octamers

Elizabeth A. Booth, Eleanor W. Vane, Dustin Dovala and Jeremy Thorner
J. Biol. Chem. published online September 28, 2015

CELL BIOLOGY

PROTEIN STRUCTURE
AND FOLDING

Access the most updated version of this article at doi: [10.1074/jbc.M115.683128](https://doi.org/10.1074/jbc.M115.683128)

Find articles, minireviews, Reflections and Classics on similar topics on the [JBC Affinity Sites](http://www.jbc.org/).

Alerts:

- [When this article is cited](#)
- [When a correction for this article is posted](#)

[Click here](#) to choose from all of JBC's e-mail alerts

Supplemental material:

<http://www.jbc.org/content/suppl/2015/09/28/M115.683128.DC1.html>

This article cites 0 references, 0 of which can be accessed free at

<http://www.jbc.org/content/early/2015/09/28/jbc.M115.683128.full.html#ref-list-1>